Characterisation and comparison of 3D printed and glass moulded optics

Indranil Basak

Master of Science Thesis
September 2015
Department of Physics and Mathematics
University of Eastern Finland

Indranil *Basak*, 50 pages
University of Eastern Finland
Master of Science Thesis
Supervisors Prof. Jyrki Saarinen
Ph.D. Kimmo Päiväsaari

Abstract

In 3D printing or additive manufacturing solid objects can be fabricated from a digital file. The Printoptical® technology is a specialized method for fabricating optics. Typically, optics is fabricated by moulding or grinding and polishing technologies, which have time and cost disadvantages. They are also limited by complex structures and they usually need post-processing. Compared to moulding or grinding and polishing technologies the Printoptical® technology can fabricate complex optics within minutes instead of weeks. It has cost advantages because no tooling is needed and it does not need post-processing.

In this work the surface quality of optics from the next generation 3D printer based on the Printoptical® technology is examined. The results are compared with previous generation equipment. We study surface roughness, surface profile, scattering, and manufacturing defects of the 3D printed optics. The quality of 3D printed optics is compared with the quality of optics, which is fabricated by glass moulding technology.

Preface

This Master of Science Thesis is part of ongoing research project '3D printed photonics - phase 1'. During my thesis work I learned a lot about 3D printing for optics. This thesis is supervised by Prof. Jyrki Saarinen and authored by Indranil Basak.

I would like to express my gratitude to my supervisors, Prof. Jyrki Saarinen and Ph.D. Kimmo Päiväsaari, who have guided me constantly during my thesis work. LUXeXceL and Oplatek are acknowledged for supplying all the samples used in this work. I wish to express my sincere thanks to Prof. Pasi Vahimaa, the head of our department. I place on record, my special thanks to Faculty of Forestry and Sciences for providing me financial support during my thesis work. I take this opportunity to express gratitude to all of the department faculty members for their help and support. I thank my parents for the encouragement, support and attention. I also place on record, my sense of gratitude to one and all, who helped me directly or indirectly.

Contents

Chapter I

Introduction

In manufacturing we typically use a tool that can fabricate objects from raw materials. The tool can convert raw materials into solid objects, which are needed in our daily life. In short, this technology makes our life simple.

Over the last two decades, industries have a focus on a class of manufacturing technologies, e.g., moulding, joining, and casting. But these technologies are limited upto certain stage. The tools cannot fabricate all kind of objects, and the cost of these tools is high. Sometimes, weeks or even months are needed to fabricate tools: the conventional processes are time-consuming. Most of the time industries are facing challenges by these conventional technologies.

Some of the limitations of manufacturing can be overcome by 3D printing or additive manufacturing. This technology can fabricate objects by adding a patterned layer upon layer. It can also fabricate complex structures. It has cost and time advantages because of no need of tooling. It introduces a new material processing technique that is known as Solid Freeform Fabrication (SFF), desktop manufacturing or fast freeform manufacturing.

The SFF technology is efficient and environmentally friendly. It follows non-contact deposition technique so that it can print on non-planer surfaces. It has a low material waste. It can fabricate complex structures and it involves with different kind of 3D printing technologies. It can even fabricate optics by inkjet printing technology.

Inkjet printing involves transferring electronic data from a computer to, e.g., paper known as two-dimensional printing. Inkjet printing is a process where a droplet of ink is ejected from a print head onto a printing medium. It is based on the process that was introduced by Lord Rayleigh in 1878, how droplets are produced from liquid stream [1]. The operating principle of inkjet device was patented in 1948 [2]. In 1971 it is demonstrated that a droplet can be created by applying a pressure wave pattern to an ink stream [3]. Inkjet printing technology was developed in the late 1970s. Small volumes of ink were ejected from a print head. But the repetition rate of the ejection was high under digital control, which increased the possibility of misprints. The printing quality is decreased by misprints. After that, the technology is developed and now it is available in office and household. Graphical printing by inkjet printing technology is valuable in the market, which means that its future is promising.

In recent years, for industrial manufacturing two-dimensional inkjet printing is converted into Three Dimentional Inkjet Printing (3DIP). It can deposit picoliter volumes of liquid as a well-defined pattern on a substrate. The printing process continues by adding a layer after layer even thousands of times to form an object. This process can produce a complex pattern by using computer-controlled translation stages and ink-dispensing. 3D inkjet printing has applications in pharmacy, chemistry or bio-chemistry, building three-dimensional (3D) objects, organic electronics, nanotechnology, and tissue engineering. As an example, the 3DIP technology is used for the manufacturing of micro-chemical parts and micro-optical parts, e.g., waveguides and micro lenses [4], polymer-light-emitting diode (PLED) displays and polymer electronics [5]. It has the following advantages: rapid prototyping, high capability, high precision dispensing, non-contact multi-material deposition, low material waste, low cost, and 3D patterning.

Nowadays, the 3D printing of optics is attractive. Printing parameters and fluid properties after the deposition are important. The fabrication of macroscopic optics by 3D printing technology is challenging. The surface quality of 3D printed optics can be improved by post-processing such as polishing or coating. But these post-processing techniques are time and money consuming. LUXeXceL [6] invented the Printoptical® technology that can fabricate optics without the need for post-

processing.

Any kind of optics cannot be used for imaging. The measurement of surface quality of optics is important for qualification. The surface roughness of optics from LUXeXceL′s previous generation equipment was 24 nm (62×47 μm^2) [7]. LUXeXceL is launching the next generation equipment. In this work the surface quality of optics from LUXeXceL's next generation equipment is investigated. The measured results are compared with previous generation equipment and imaging optics quality. In this thesis we also characterize and compare 3D printed optics from LUXeXceL and glass moulded optics from Oplatek [8].

In Chapter II different kind of additive manufacturing technologies, which can fabricate solid objects are introduced. Different kinds of inkjet printing processes, fluid properties and challenges for inkjet printing are considered in Chapter III. Chapter IV describes characterisation methods for 3D printed optics. In Chapter V surface roughness, surface waviness, and scattering of 3D printed optics and glass moulded optics are measured and compared. Conclusions are presented on Chapter VI. Future work is outlined on Chapter VII.

Chapter II

3D printing technology

In this chapter different kind of 3D printing technologies followed by Solid Freeform Fabrication (SFF) are described.

2.1 Solid Freeform Fabrication

Solid Freeform Fabrication (SFF) is used to fabricate solid prototype models by taking information from 3D modelling software, e.g., a Computer-Aided-Design (CAD) file. Designers can check the function and appearance of these prototypes before fabrication. In the first step of SFF the design of a prototype is created by using a modelling programme followed by sending the design to a CAD software. The software will break the design into hundreds or thousands of thin layers. The prepared file is further sent to the machine that fabricates designed model by adding a patterned layer upon layer (Fig. 2.1). The main two advantages of the process are: (1) giving designers more freedom that they can draw their design more efficiently and (2) low material waste.

Nowadays, different kind of SFF technologies are available in the market. SFF can fabricate complex parts by common stock materials, e.g., liquid, powder, and thermoplastics. SFF technology includes stereolithography (SLA), fused deposition modelling (FDM), selective laser sintering (SLS), three-dimensional inkjet printing (3DIP) etc. In SLA technology complex photopolymer shapes are fabricated by using light to solidify selective portion of liquid photocurable resins. In SLS technology, powder is used as raw material and powdered layers are sintered selectively by laser. The material for FDM technology is thermoplastics and it is melted above

its melting point to create a layer, which solidifies by natural cooling. In 3DIP technique, objects are fabricated by the deposition of ink-jets.

2.1.1 Selective Laser Sintering (SLS)

In the first step of the SLS process, to create a layer, powder material is spread out and levelled onto the surface of a support stage. A portion of layer is selected by 3D modelling software and it is fused by high energy laser. After the first layer is fabricated, the support stage moves downward at a distance, which is the thickness of the fabricated layer. The next layer is constructed above the fabricated layer by similar process and by adding a layer upon layer the process continues until the object is built. All subsequent layers are fused together by laser energy. After the object is fabricated, it is separated from loose powder (Fig. 2.2).

In SLS process the final object consist with borders due to laser sintering of high melting point. The surface quality of the final object must be improved by post-processing. Another disadvantage of this technique is that parts in the machine take a long time for cooling [9].

2.1.2 Fused Deposition Modelling (FDM)

In FDM technology powder is used as raw material. It is mixed with thermoplastic polymer or wax binder. By mixing, granulating, and extruding with rollers, the materials are made flexible and continuous. It is brought up into a movable and heated nozzle to melt it above its melting point. The print-head moves and ejects material according to the shape of the layer, which is created by 3D modelling software. The layer solidifies by natural cooling and every next layer makes a bond with previous layers. Adding a layer upon layer process continues until the 3D object is built (Fig. 2.3).

The surface quality of the fabricated part is not good enough for high-quality applications before post-processing due to internal defects. These defects occur because of poor bonding between layers [10, 11].

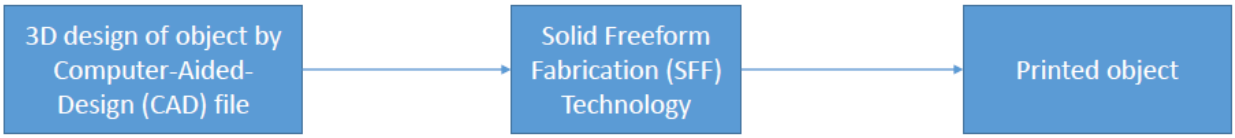

Figure 2.1: Schematic drawing of Solid Freeform Fabrication (SFF).

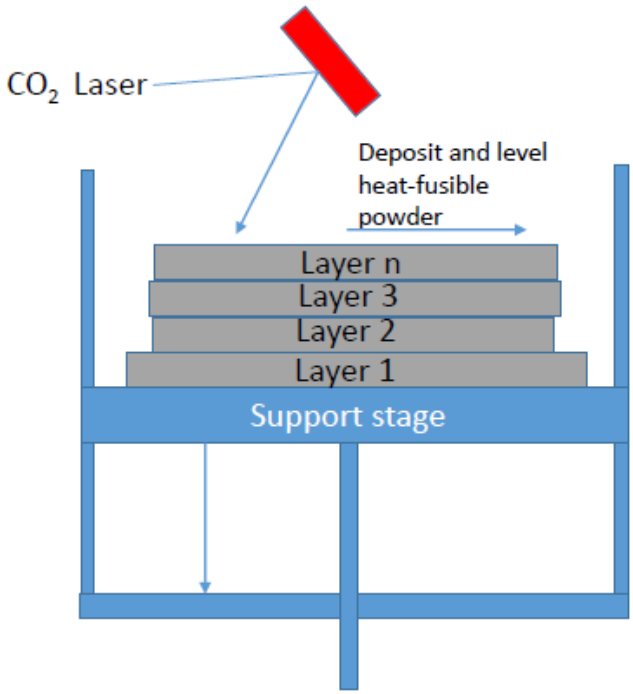

Figure 2.2: Schematic drawing of the Selective Laser Sintering (SLS) process.

2.1.3 Stereolithography (SLA)

In Stereolithography (SLA) at the first step liquid chamber is filled with liquid monomer. The support platform enters into the liquid chamber to create the first thin liquid monomer layer. The layer is polymerized by ultraviolet (UV) radiation from a laser. The support platform moves downward to create next thin liquid monomer layer above the first fabricated one. Recoat blade moves across the liquid surface to make the desired thickness of the next layer. The next layer is polymerized by similar way and adding a layer upon layer process continues until the final 3D object is built. The support platform is raised up to remove the final object from the support platform (Fig. 2.4) [12].

The typical 3D printer based on SLA's technology cannot be used to print optics because objects consist of borders. When next layer start to fuse with previous layer, the border arises. The surface roughness of final part increase because of the borders.

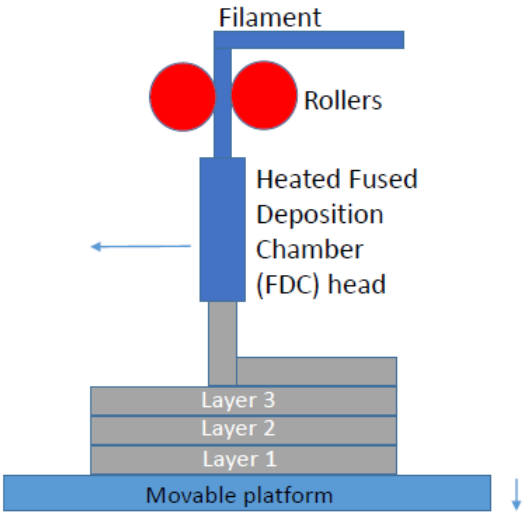

Figure 2.3: Schematic of Fused Deposition Modelling (FDM) apparatus.

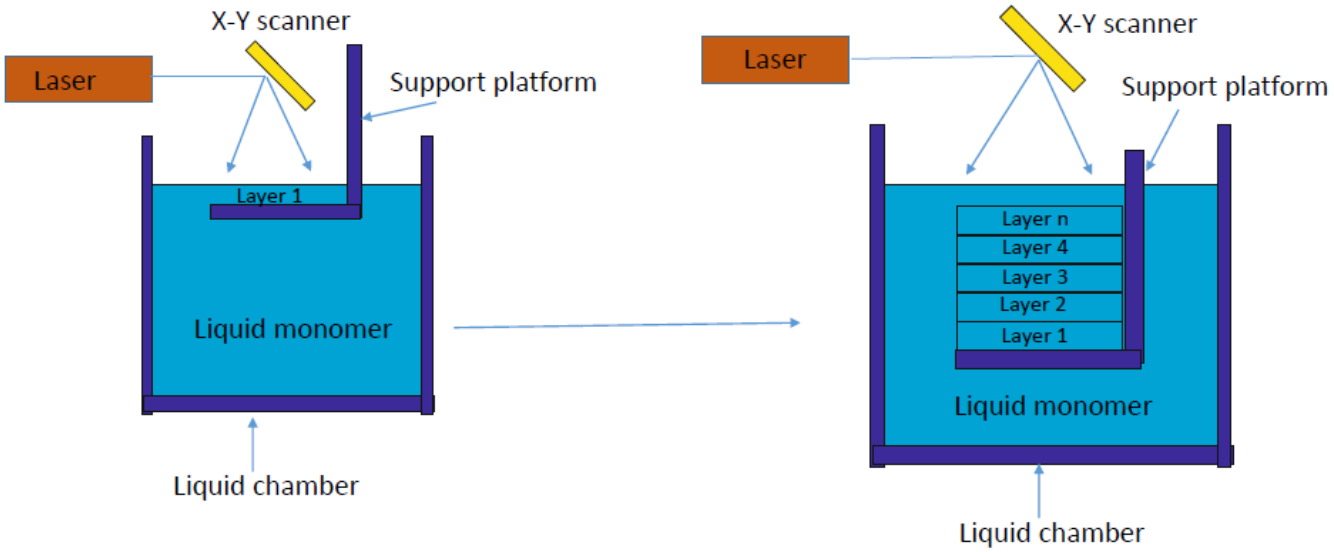

Figure 2.4: Working process of a 3D printer based on Stereolithography (SLA) technology.

Chapter III

Ultraviolet (UV) curable inkjet printing

The fabrication of optics by 3D printing technology is challenging. The optics can be fabricated by UV curable inkjet printing technology. So this chapter has focus on inkjet printing technology and material properties of UV curable inkjet printing technology. In UV curable inkjet printing droplets are created from the stream of ink. They are ejected from a computer controllable moving print head and deposited on a substrate. Liquid has connecting property that is called surface tension of a liquid. For example, when two small droplets connect with each other, it will form a big droplet. Based on this principle, deposited droplets on the substrate connects with each other and form a continuous patterned layer that is polymerized by UV light. A printing stage moves downward at a distance which is equal to the thickness of the first layer. Then next layer is fabricated above the first layer and by adding a layer upon layer the process continues until the 3D object is built (Fig. 3.1).

Inkjet printing is classified by continuous inkjet printing and drop-on-demand (DOD) inkjet printing [13, 14].

3.1 Continuous inkjet printing

In continuous inkjet printing droplets are ejected from the print head continuously. The continuous inkjet printer can be classified by binary deflection system and multiple deflection system.

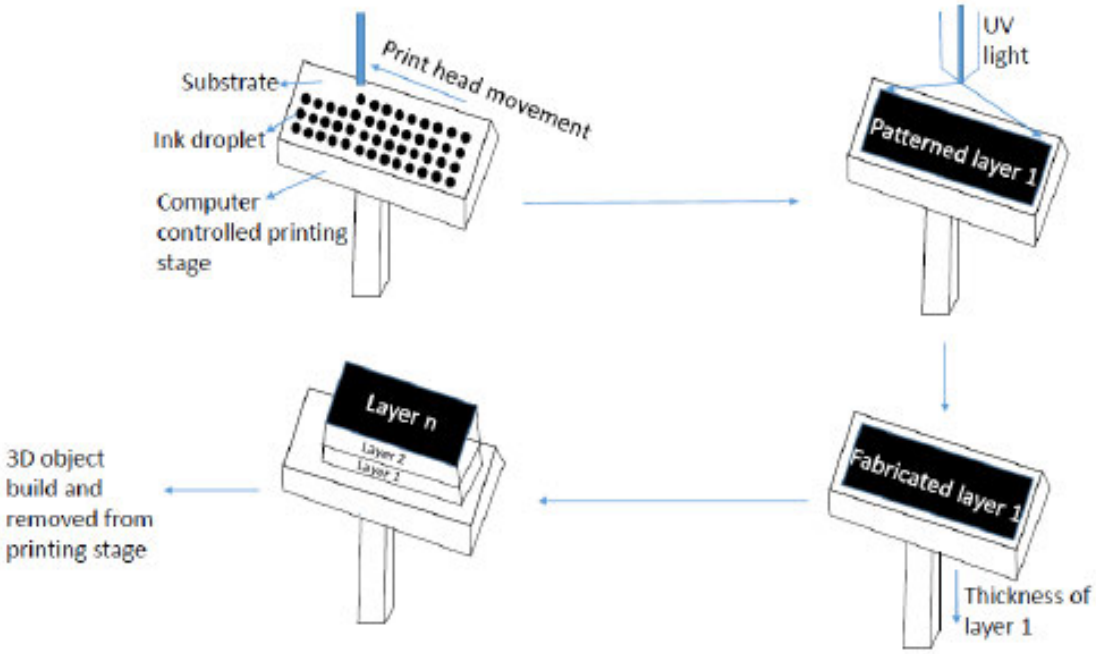

Figure 3.1: Diagram of ultraviolet (UV) curable inkjet ptinting.

3.1.1 Binary deflection system

Figure 3.2 shows continuous stream of ink that is piezoelectrically pulsed and ejected from a drop generator. It passes through a charge electrode and breaks into droplets that are either charged or uncharged. Uncharged droplets fly straight and they are deposited on the substrate. The charged droplets are deflected by a high voltage deflection plate and collected by a gutter for recycling.

3.1.2 Multiple deflection system

The operating principle of a multiple and binary deflection system is same but in the former one charged droplets are deflected by a high voltage deflection plate and deposited onto the substrate at different positions. The uncharged droplets fly straight and they are collected by a gutter for recycling (Fig. 3.3). Continuous inkjet printers are used for high speed printing, e.g., bar codes, and sell-by dates.

Surface quality from continuous inkjet printing system is not good enough for optics because the user does not have control on droplets as droplets are ejected continu-

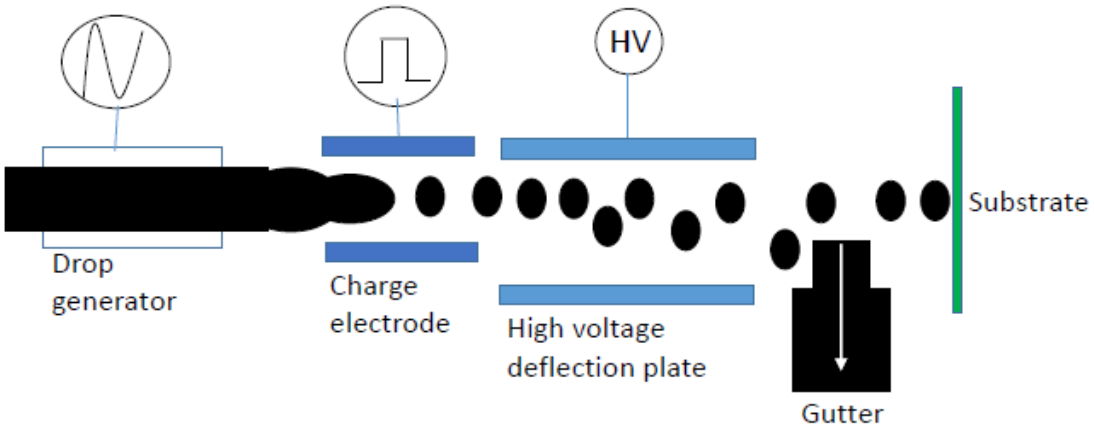

Figure 3.2: Binary deflection system.

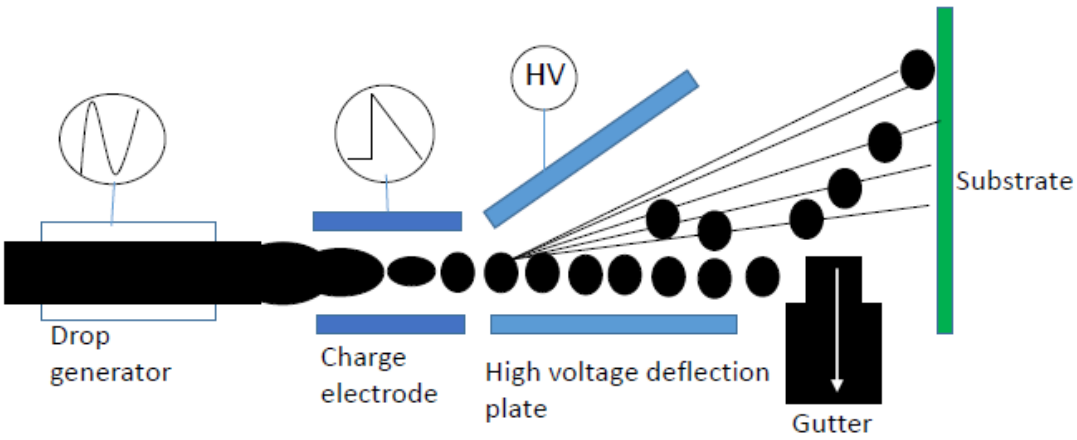

Figure 3.3: Multiple deflection system.

ously from the print head. The probability of drop deposition at unwanted positions is high, which increases the possibility of misprinting. The surface quality is decreased by misprints (see Section 3.4).

3.2 Drop-on-demand (DOD) inkjet printing

In drop-on-demand (DOD) inkjet printing a droplet is ejected from a print head only when it is required for printing. Five types of DOD inkjet printers are available: piezoelectric, thermal, electrohydrodynamic (EHD), cavity collapse, and acoustic inkjet printing.

3.2.1 Piezoelectric DOD inkjet printer

The nozzle for the piezoelectric DOD inkjet printing technology is fabricated from piezoceramic materials. There are three types of piezoelectric DOD inkjet printers: squeeze mode actuator, bend mode actuator, and push mode actuator [15]. The operating principle of the actuators is following:

Squeeze mode actuator: The print head is fabricated from a piezoelectric ceramic tube. The transducer is connected to the outer surface of the tube. The droplet is ejected from the orifice, when a short rise time voltage pulse that causes contraction of the tube, is applied to the transducer (Fig. 3.4).

Bend mode actuator: A diaphragm is attached to one side of a pressure chamber. A piezo-ceramic plate is attached to the diaphragm. The outer surface of the plate consists of conductive coating that transfers electrical connection to the plate. When a voltage is applied to piezo-ceramic plate, it contracts and it causes diaphragm to move inside the pressure chamber. Due to the internal pressure, droplet will be ejected from an orifice (Fig. 3.5). Droplet size depends on orifice diameter, voltage of the pulse, and pulse duration [16].

Push mode actuator: Figure 3.6 shows that when a voltage pulse is applied to a piezo-ceramic rod, it contracts and pushes diaphragm inside a pressure chamber. Due to the internal pressure, droplet will be ejected from an orifice. A thin diaphragm prevents unwanted interaction between ink and ceramic rod.

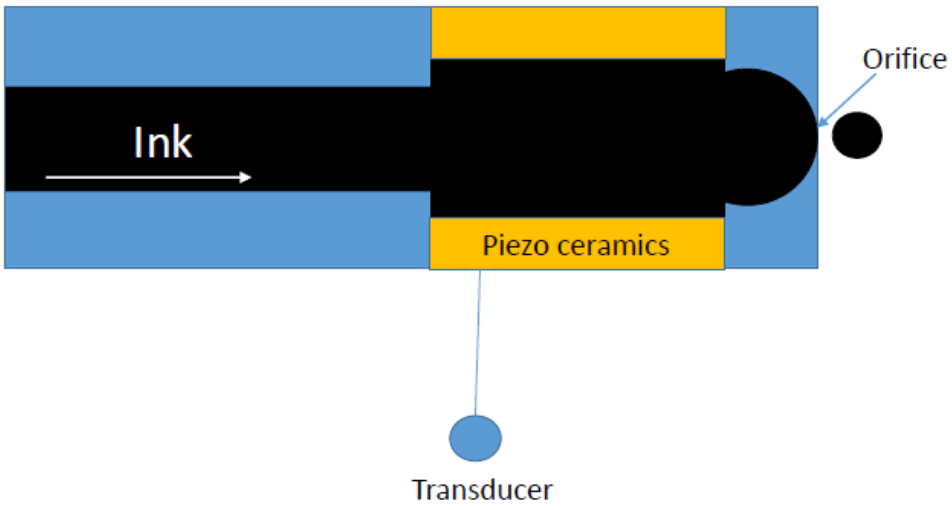

Figure 3.4: Diagram of squeeze mode actuator.

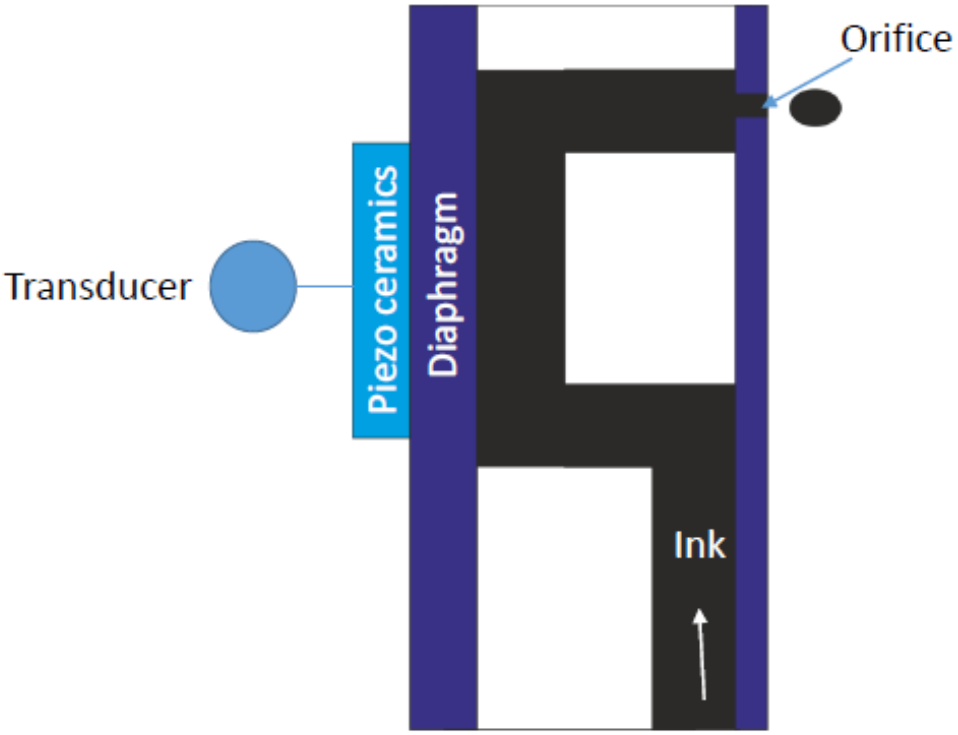

Figure 3.5: Diagram of bend mode actuator.

3.2.2 Thermal DOD inkjet printer

In a thermal drop-on-demand inkjet printer, when voltage pulse is applied to a heater, ink is superheated and it achieves its critical temperature for bubble nucleation (Fig. 3.7). The bubble starts to expand and force the ink out from a orifice. When the temperature starts to diminish, bubble begins to collapse and create a droplet that is deposited on a substrate. Because of capillary force, ink chamber will be refilled and the process can be started again [13].

The droplet and nozzle diameters are identical for piezoelectric and thermal DOD inkjet printing technology. But smaller droplet from larger nozzle diameter can be achieved by using the following processes:

3.2.3 Electrohydrodynamic DOD inkjet printing

Liquid can be drawn from a nozzle when electric field is applied to the liquid [17–20]. Figure 3.8 shows that electric field applied to the liquid, creates a Taylor cone at the tip of an orifice. A droplet is ejected from the tip of the Taylor cone.

3.2.4 Cavity collapse DOD inkjet printing

Cavity collapse can be used to achieve a Worthington jet from a large nozzle [21,22]. Figure 3.9 shows that when negative pressure is applied to ink, a cavity is created. The cavity is converted into collapse by changing negative pressure into positive pressure. Therefore, a thin jet eventually breaks up from violent collapse and a droplet is created. The diameter of droplet is smaller than the nozzle diameter [21].

3.2.5 Acoustic DOD inkjet printing

Figure 3.10 shows piezoelectric transducer attached to one end of a buffer rod. The other end is connected to an acoustic lens, which is filled with ink. Sound wave is generated from the buffer rod when radio frequency (rf) pulse is applied to a transducer. The sound wave propagates towards the acoustic lens that focuses on the surface of the ink. The sound wave is transmitted by the acoustic lens and a droplet is ejected from the surface of the ink. High energy of the sound wave is needed to eject a droplet from the surface of the ink [23].

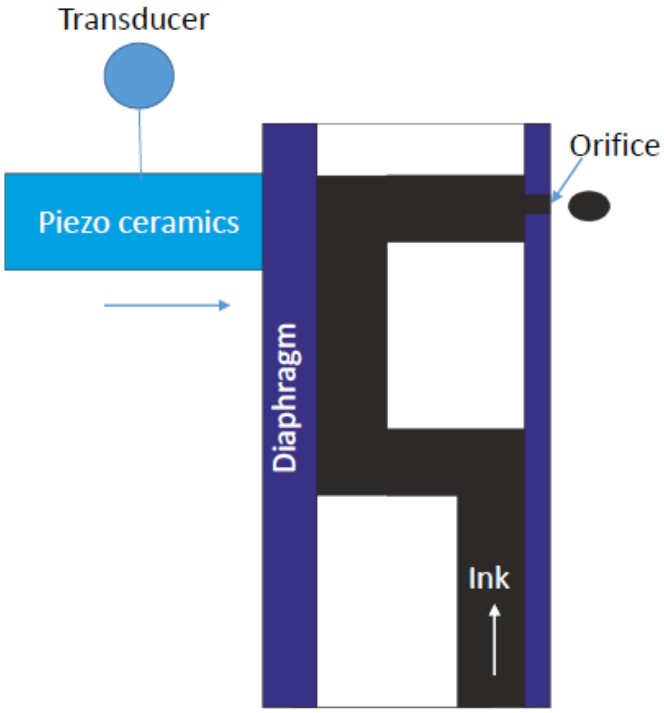

Figure 3.6: Diagram of a push mode actuator.

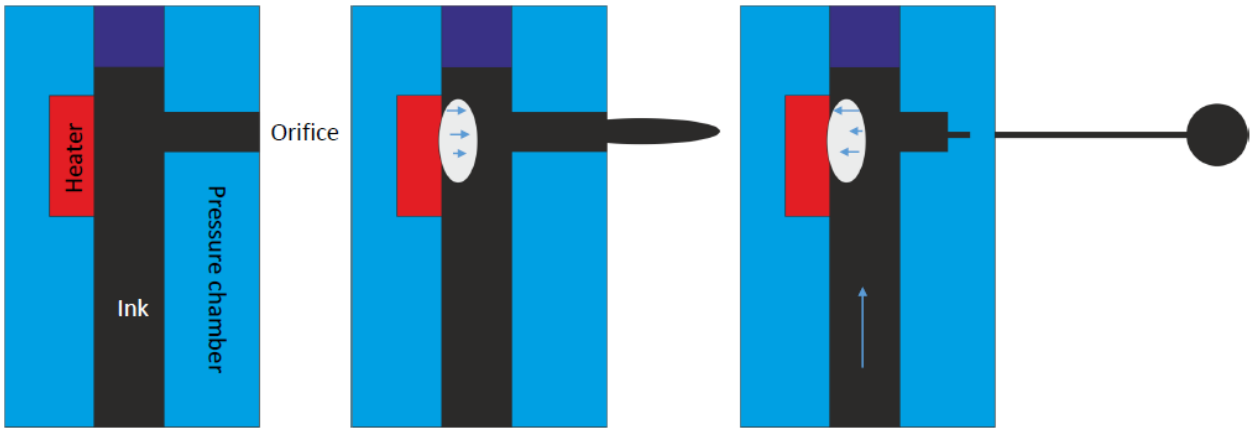

Figure 3.7: Diagram of thermal DOD inkjet printing.

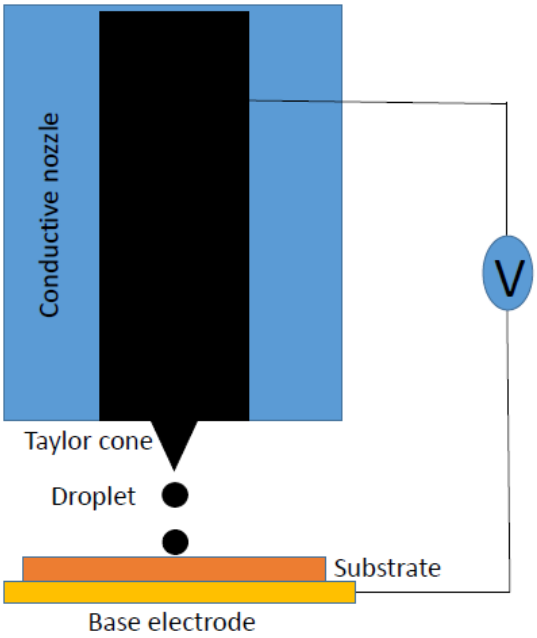

Figure 3.8: Diagram of electrohydrodynamic DOD inkjet printing technology.

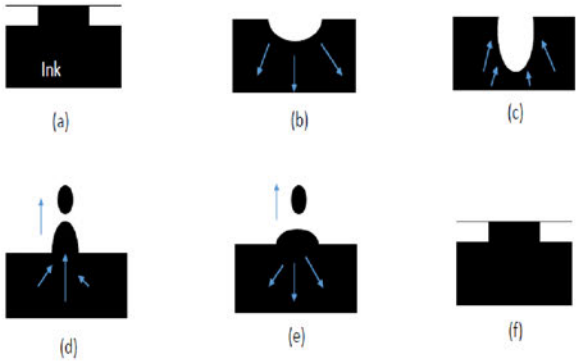

Figure 3.9: Diagram of cavity and collapse DOD inkjet printing technology: (a) liquid surface is in steady state, (b) cavity is created by negative pressure, (c) extended collapse, (d) droplet is produced from collapse by positive pressure, (e) collapse retracts, and (f) liquid surface regains initial state.

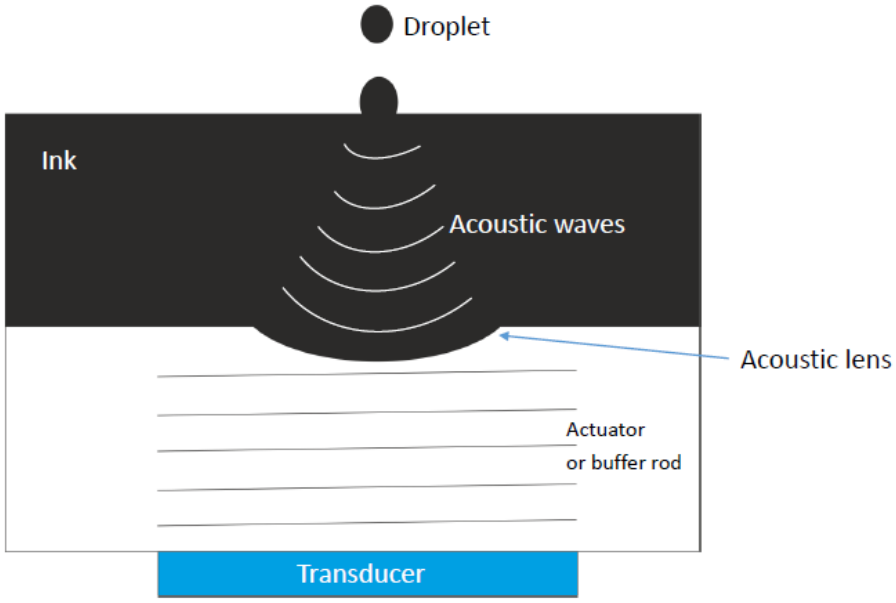

Figure 3.10: Diagram of acoustic DOD inkjet printing technology.

3.3 Ink properties of DOD inkjet printing

Formation of drops from the stream of ink is complex. The properties of a drop depend on a number of dimensionless constants: Reynolds (Re), Weber (We), and Ohnesorge (Oh) numbers

$$Re = \frac{v\rho a}{\eta} \tag{3.1}$$

$$We = \frac{v^2\rho a}{\gamma} \tag{3.2}$$

$$Oh = \frac{\sqrt{We}}{Re} = \frac{\eta}{\sqrt{\gamma\rho a}} \tag{3.3}$$

where ρ, η, γ, v, and a are the density, kinematic viscosity, surface tension, velocity, and drop diameter, respectively.

Drop formation is characterized by the Ohnesorge number, which was identified by Fromm [24]. He proposed that for stable drop generation $Z > 2$, where $Z{=}1/Oh$. The work was rechecked by Resis and Derby. They used numerical simulation of drop formation and proposed that $10 > Z > 1$ for stable drop generation [25]. At

high values of Z, ejected drop connects with a large number of satellite droplets and for small values of Z, viscous dissipation does not allow drop ejection from an orifice. The surface tension prevents liquid to eject from the nozzle. The barrier can be overcome by the minimum velocity v_{min}.

$$v_{min} = \left(\frac{4\gamma}{\rho d_n}\right)^{\frac{1}{2}} \tag{3.4}$$

where d_n is the nozzle diameter.

For imaging optics, surface roughness is an important issue. The relation between *We*, *Re* and *f(R)* was first proposed by Stow and Hadfield [26].

$$We^{\frac{1}{2}} Re^{\frac{1}{4}} > f(R) \tag{3.5}$$

where *f(R)* is the function of surface roughness.

For flat and smooth surfaces $f(R) \approx 50$ [27]. Typically, for imaging application the limit of root-mean-square roughness is as low as 5 nm. *f(R)* especially depends on γ and η.

According to Young's equation the surface free energy of solid (substrate) is defined by

$$\xi_s = \xi_{sl} + \gamma \cdot cos\theta \tag{3.6}$$

where ξ_{sl} is the interfacial tension between solid and liquid, and θ is the contact angle between drop and solid (Fig. 3.11). The surface quality of optics can be improved by proper θ. If ξ_s is higher than γ, then θ improves. Poor γ causes poor contact between ink and inner surface of nozzle. The drop ejects from the nozzle spontaneously, which increases the possibility of misprints.

There have two types of fluid: Newtonian and Non-Newtonian. Newtonian fluid is used as printing material because of low η, which makes the droplet surface smooth. Furthermore, research is necessary to use Non-Newtonian fluid as printing material.

Two other major factors to improve surface quality are ρ and a. Droplets are spattered on a substrate because of the distance between the print head and the

substrate. Higher ρ prevents spattering and produce droplet with proper shape. Small a and proper distance between deposited droplets improve surface quality.

3.3.1 Drop behaviour and spreading

Drop behaviour on a solid surface depends on inertial forces, capillary forces, and gravitational forces. The gravitational force depends on an important dimensionless parameter, called bond number B_0.

$$B_0 = \frac{\rho g a^2}{\gamma} \tag{3.7}$$

where g is the gravitational force.

Typically, fluid density 1000 kg/m^3, surface energy below 0.1 J/m^2, and drop density below 100 μm is used for inkjet printing. Because of high surface energy $B_0 << 1$, gravitational forces can be neglected. Yarin [28] used a fluid that v range was 1-30 m/s, and a range was 100-3000 μm, to check drop behaviour on the substrate. He examined that the diameter of the droplet increases with respect to time (Fig. 3.12). Dimensionless time after impact is defined by

$$t = t_0 \frac{v}{a} \tag{3.8}$$

where t_0 is the initial time [29].

For small values of t (e.g., t=0.1), surface tension plays an important role to control the drop, and viscous force prevents oscillation and spreading. At larger values of t, droplet diameter a, which is controlled by capillarity, increases [30]. Contact diameter (d_{con}) of the final drop is defined by

$$d_{con} = a \sqrt[3]{\frac{8}{tan\frac{\theta_{eqm}}{2}(3 + tan^2\frac{\theta_{eqm}}{2})}} \tag{3.9}$$

where θ_{eqm} is the equilibrium contact angle ($d_{con} \approx 3a$ for $\theta_{eqm} = 10^0$).

The final drops connect with each other to form a patterned layer.

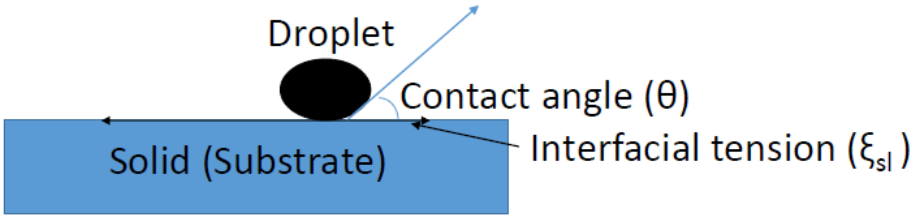

Figure 3.11: Diagram of contact angle.

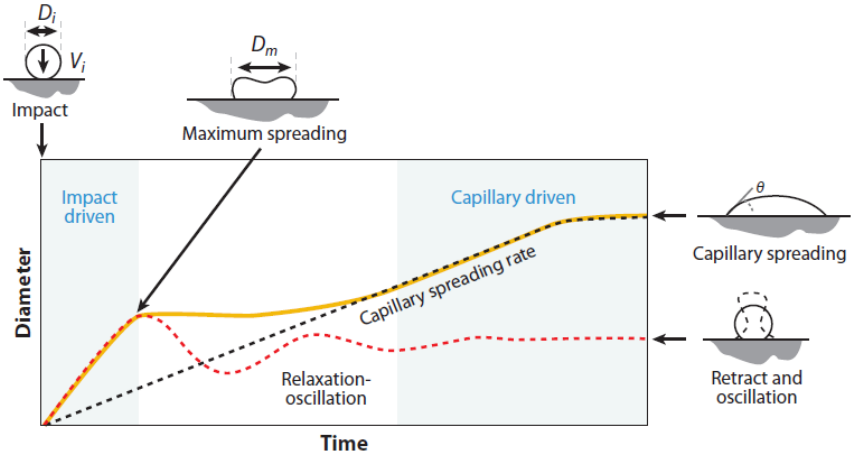

Figure 3.12: Schematic illustration of droplet impact on a substrate [31].

3.3.2 Pattern stability

Davis [32] proposed that fluid line on a flat surface is stable if the contact line (Fig. 3.13) between them is fixed and the contact angle is $<\pi/2$. The proposal was confirmed experimentally by Schiaffino and Sonin [33]. Liquid beads on a flat surface are formed by overlapping of drops. If drops do not overlap with each other, then it is impossible to form liquid beads. Overlapping of drops is possible by the appropriate contact line between drops. Davis [32] predicted that constant contact angle causes unstable contact line and this prediction was observed by Schiaffino and Sonin [33]. If the contact angle consists of hysteresis, then a stable contact line can be printed that form parallel liquid bead, but sometimes bulges are observed. Duineveld [34] proposed that, when a newly deposited drop interact with liquid bead, bulging stability occurs. Figure [3.14 (a)] shows that drops do not interact with each other, if the drop spacing is large. Drops overlap with each other if the drop spacing is slightly smaller than the diameter of a footprint, but in that condition liquid beads are not parallel [Fig. 3.14 (b)]. The liquid bead will be stable by proper spacing of deposited drops [Fig. 3.14 (c)]. If the spacing between deposited drops are too small, bulging instability occurs, which mainly depends on drop spacing and printing speed [Fig. 3.14 (d)].

3.4 Surface quality of printed optics

In addition to material properties, the quality of 3D printed optics is defined by resolution that depends on a number of dots/m^2. It is important to connect all droplets together to form a continuous 3D body with smooth surfaces. Surface quality can be improved by inserting small drops in between large drops, and reducing the large drop diameter. If the positions of drops are not in the right place, point defects can be observed.

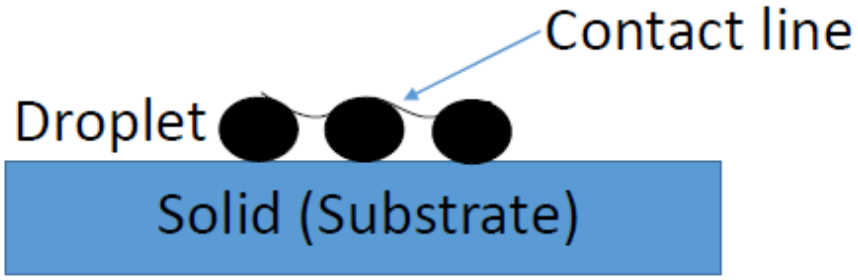

Figure 3.13: Diagram of contact line.

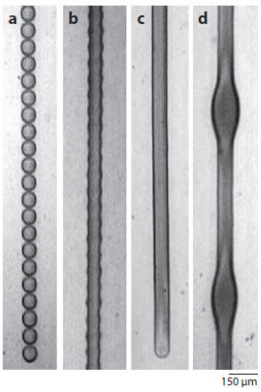

Figure 3.14: Schematic illustration of pattern at different drop spacing [35].

Chapter IV

Characterisation methods

LUXeXceL′s Printoptical® technology is further development of UV curable inkjet printing (Fig. 4.1). The major advantage of this technology is that final object does not consist of borders. Without any post-processing it can produce objects with smooth surface quality. The surface quality of 3D printed optics is measured by WYKO NT9300 Optical Profilometer. The profile of 3D printed and glass lenses are observed by 4F imaging and scattering measurement set-ups.

4.1 WYKO NT9300 Optical Profilometer

WYKO NT9300 is a vertical scanning interferometer and it can be used to measure the surface roughness of object. It can operate in phase shifting interferometry (PSI) and vertical scanning interferometry (VSI) modes. It is a cost-effective instrument that has an easy setup, fast data acquisition, and comprehensive analyses. It has a sub-ångstrom resolution in PSI mode and nanometer resolution in VSI mode. It is controlled by vision software.

WYKO NT9300 operates by the principle of Michelson or Mirau interferometer. The interference fringes are observed when the path difference of interfering wave is identical. Before starting measurements in PSI mode, field background correction is needed. This correction can be done by calibrating the instrument with a reference optics of flatness 1.25 Å. The relation between optics movement and fringe phase shift is measured by PSI calibration. Similarly, VSI calibration measures the relation between optics head movement and achieved step height. After the calibration, reference optics is replaced by 3D printed sample and interference fringes are observed.

WYKO NT9300 has systematic measurement errors due to photon shot noise, thermal current, thermal noise, readout noise, quantization noise, background errors, bias, and miscellaneous errors. The systematic errors can be removed by appropriate corrections (e.g., reference frame). Non-systematic errors can be removed by averaging. The optical specification of WYKO is shown in Table 4.1. The picture of WYKO NT9300 optical profilometer is shown in Fig. 4.2.

The measurement with optical profilometer is beneficial compared to an atomic force microscope and a diamond stylus. An atomic force microscope has long exposure time. It takes several hours for measurement of a small portion of the surface. The needle diameter of a diamond stylus is required in nano-meter (nm) region to observe surface quality of 3D printed sample. The needle with such small diameter hits and makes scratches on sample surface.

TABLE 4.1
Optical specification of WYKO NT9300 Optical Profilometer.

	Objective		
Optical specification	2.5×	10×	50×
Numerical aperture	0.07	0.30	0.55
Optical resolution	3.8 μm	0.89 μm	0.49 μm
Working distance	3.5 mm	7.4 mm	3.4 mm
Objective type	Michelson	Mirau	Mirau

The surface of macroscopic optics can be considered smooth if $\delta_q << \lambda$, where δ_q is root-mean-square (rms) roughness and λ is the wavelength, which is illuminated on the surface (Fig. 4.3) [37]. The optics surface will have high surface roughness value if it consists with waviness. But surface roughness can be diminished by applying filter to the surface (Fig. 4.4).

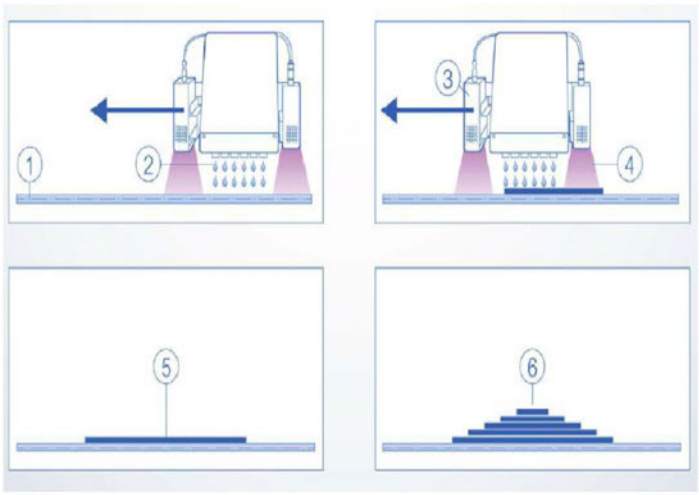

Figure 4.1: Schematic representation of Printoptical® technology [36] (1- substrate, 2- drops from nozzle, 3- UV lamp, 4- UV light, 5- one layer, 6- several layers).

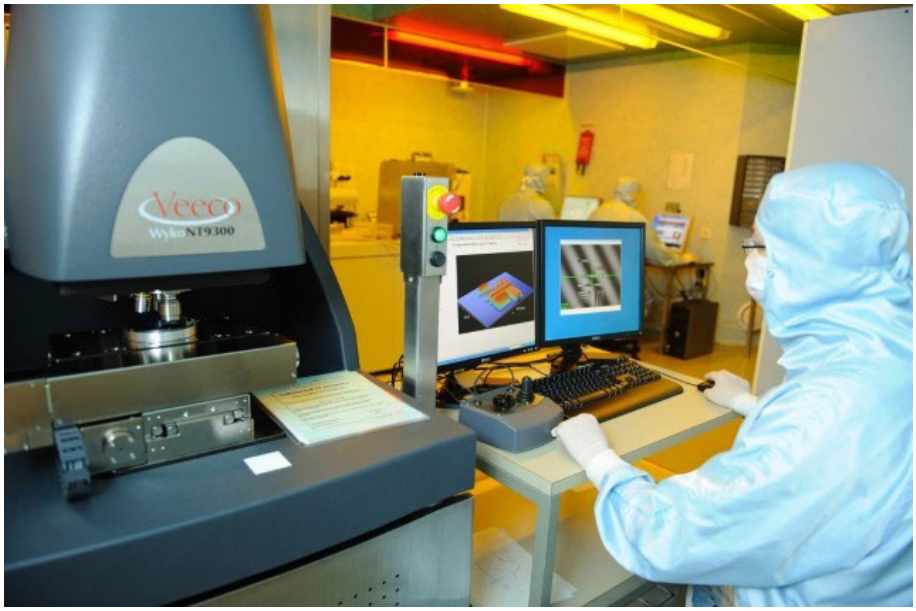

Figure 4.2: WYKO NT9300 Optical Profilometer.

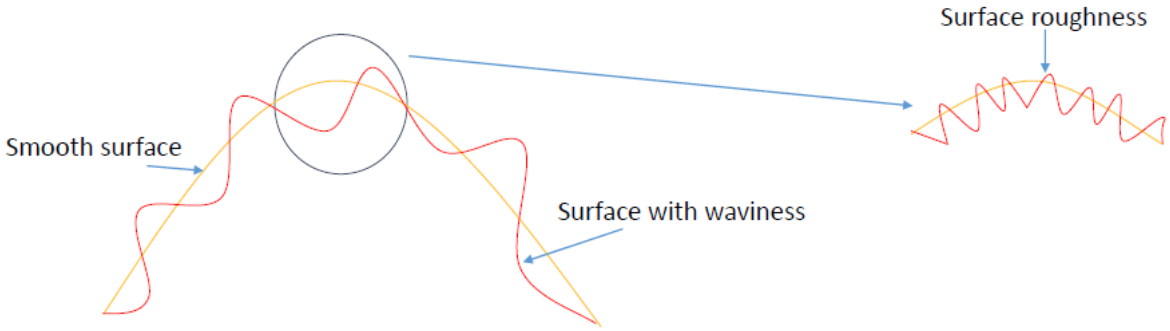

Figure 4.3: Diagram of the optics surface.

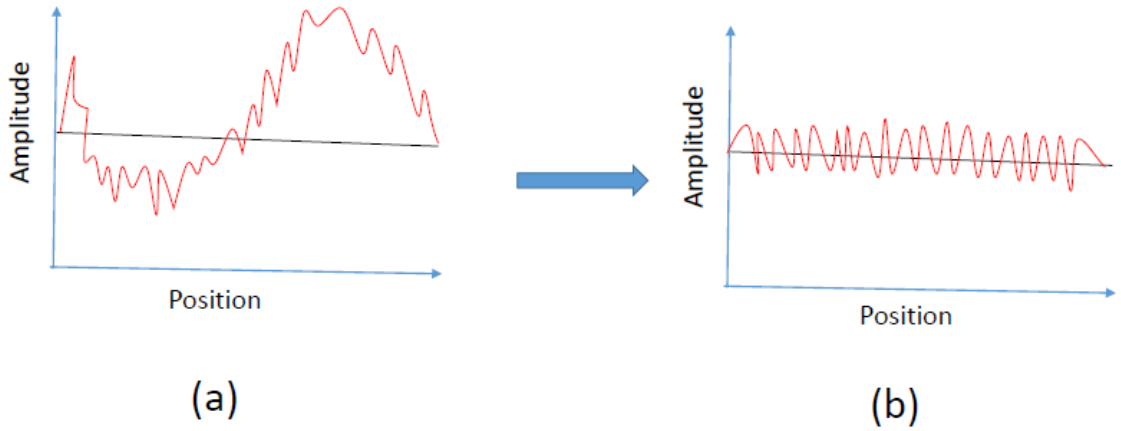

Figure 4.4: Diagram of the optics surface (a) without filter, (b) with filter in order to remove surface waviness.

4.2 4F imaging

The 4F imaging system is used to create a real image of an object. The f/number of a lens is defined by

$$N = \frac{f}{D} \tag{4.1}$$

where f is the focal length and D is the diameter of the lens. The quality of an image depends on N. Lenses with smooth or rough surface have focal point or spot (Fig. 4.5). The focal length cannot be measured from the focal spot. Lenses with focal spot have poor imaging quality that can be observed by the 4F imaging system (see Section 5.2).

4.3 Scattering

Scattering of light is a process in which light incidents on an object and scattered. It can be considered as the deflection of light from a straight path. The light scatters by the smooth surface is identical, so the scattered light is uniform. But in case of rough surface it is non-uniform. The surface quality of optics can be understood by the quality of scattered light (e.g., uniform or non-uniform) (see Section 5.3).

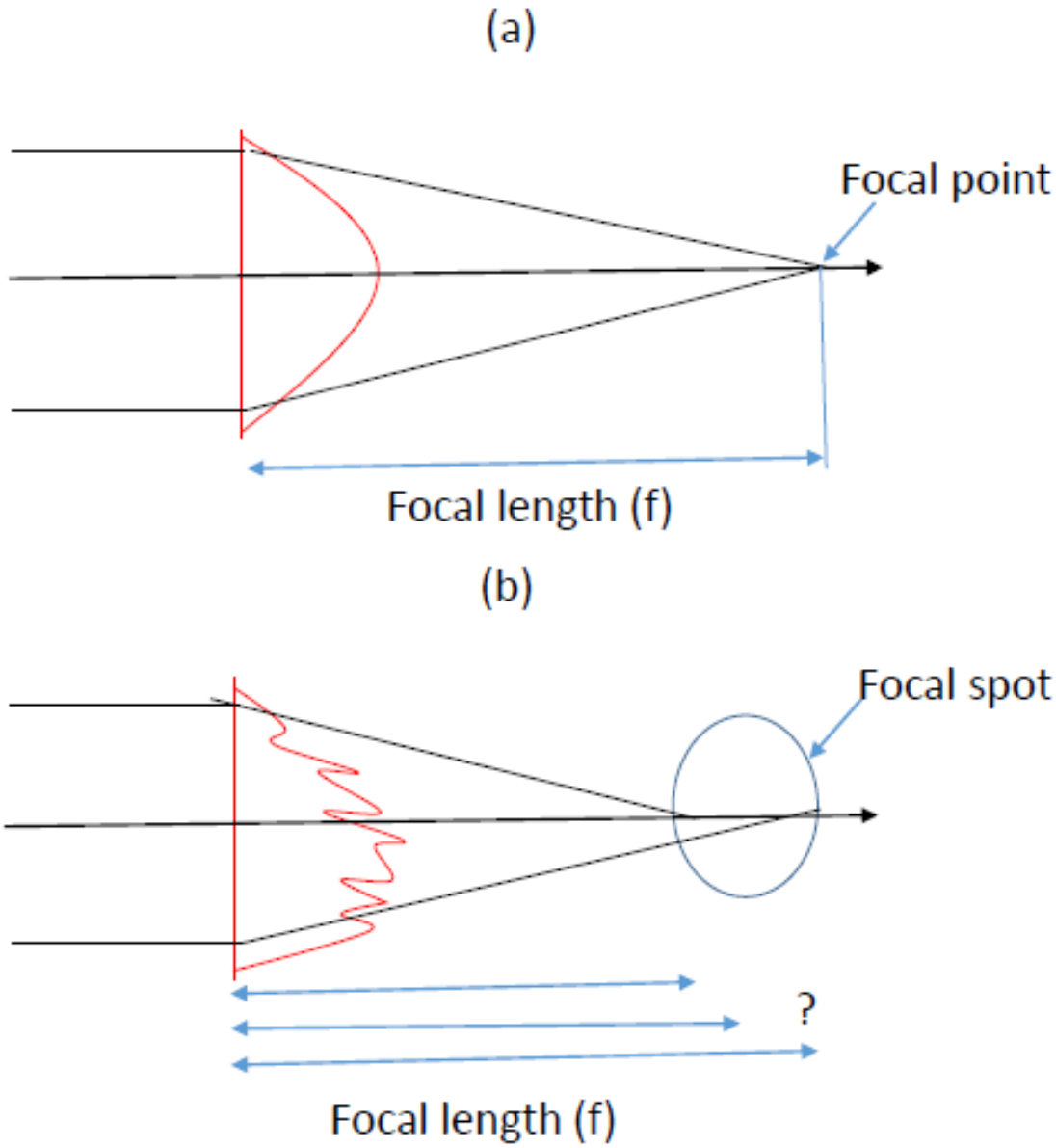

Figure 4.5: Diagram of focal length for a lens with (a) smooth surface and (b) rough surface.

Chapter V

Experiments

In this chapter 3D printed optics by LUXeXceL and moulded glass optics by Oplatek were characterized. 3D printed optics was fabricated by UV curable piezoelectric drop-on-demand inkjet printing technology (see Section 3.2). Surface roughness, surface waviness and scattering of light were investigated. The samples printed by LUXeXceL is shown from Figs. B.1 to B.6.

5.1 Surface roughness

The surface roughness of 3D printed optics and glass moulded optics was measured by WYKO NT9300 optical profilometer [38]. Before the measurements all samples were cleaned properly with dilute water. Then the samples were dried by high pressure nitrogen gas to remove dust particles from the surface of the samples. Alcohol was not used because it can melt the 3D printed samples.

The optical profilometer has phase-shifting-interferometry (PSI) and vertical-scan-interferometry (VSI) modes. In our measurement PSI mode was used (see Section 4.1). The resolution of an image in VSI mode was too poor. The tilt and curvature of the samples were removed from measurement data. The approximate size and thickness of 3D printed flat samples were 2×1.5 cm^2 and 2 mm, respectively. Both of the surfaces were flat and these samples were printed on December, 2014 (Fig. 5.1). Measured surface roughness of the 3D printed flat samples are shown in Tables 5.1 and 5.2, where δ_a is area roughness. As 3D printed surface consists with waviness, roughness value increases with evaluation area (Tables 5.1 and 5.2). Photographs of the surfaces are shown in Figs. 5.2 and 5.3.

The surface roughness values are high in Tables 5.1 and 5.2 because 3D printed surface has also waviness. The waviness can be removed from the surface roughness measurement by using filtering with specific cutoff wavelength. The cutoff wavelength was chosen using DIN EN ISO 4288, ASME B46.1 standard. After removing waviness from the measured data the surface roughness values were improved. The measured surface roughness with filter are shown in Tables 5.3 and 5.4.

The surface rms roughness value of optics by LUXeXceL's previous generation equipment was 24 nm (62×47 μm^2). But now the quality is improved and it is close to 5 nm (62×47 μm^2). The surface of 3D printed optics by LUXeXceL's previous generation equipment consisted with point defects (e.g., bumps, nipples, and snowflakes) [7]. But point defects are removed by LUXeXceL's next generation equipment.

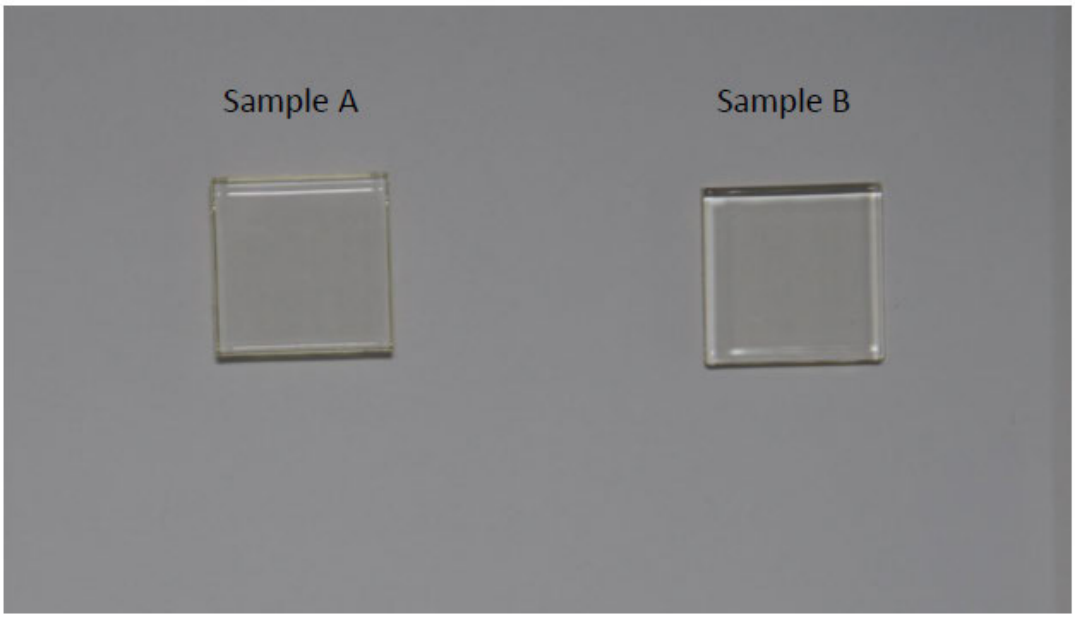

Figure 5.1: Photographs of 3D printed samples.

The design of both 3D printed and glass moulded prisms were similar and they were not polished. One of the prism surface consisted with gratings and rest of the surfaces were flat, which were measured by WYKO NT9300. Approximate length,

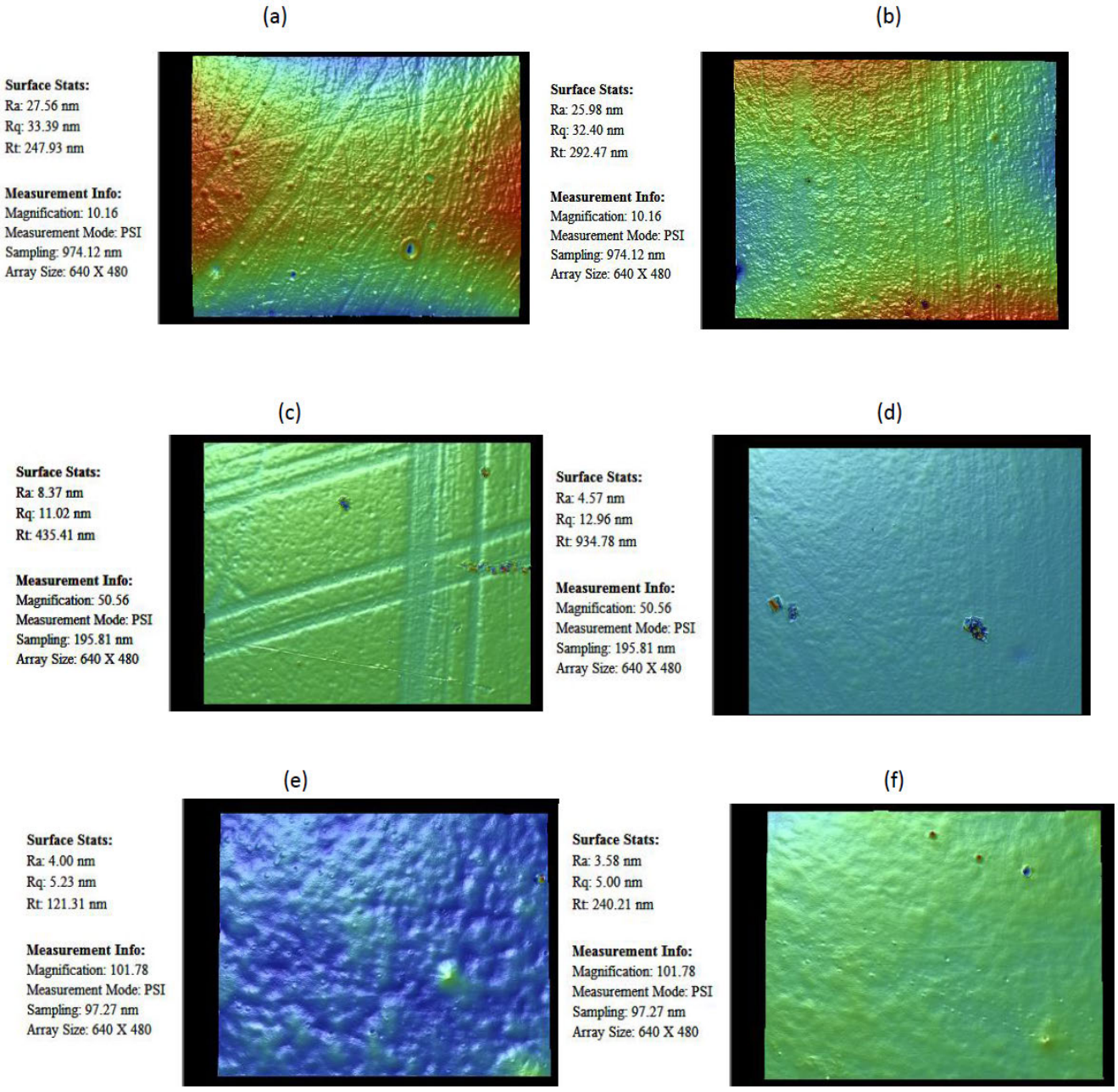

Figure 5.2: Photographs of 3D printed flat sample A by WYKO NT9300 at evaluation area (a,b) 622×467 μm^2, (c,d) 125×94 μm^2, and (e,f) 62×47 μm^2.

TABLE 5.1

Surface roughness of the 3D printed flat sample A, where σ and σ_m are the standard deviation and mean of the standard deviation, respectively.

Evaluation area in μm^2	Roughness in nm without filter					
	622×467		125×94		62×47	
Number of observation	δ_a	δ_q	δ_a	δ_q	δ_a	δ_q
1	52.5	65.3	4.8	9.7	2.6	5.3
2	36.1	44.5	20.7	36.7	4.2	5.8
3	26.0	32.4	4.6	13.0	3.6	5.0
4	49.0	61.1	4.2	5.5	6.2	8.3
5	27.6	33.4	3.5	4.6	4.0	5.2
6	23.4	30.0	3.7	8.1	3.6	6.3
7	36.4	47.3	8.4	11.0	2.3	3.1
8	40.3	49.5	7.8	9.5	4.0	5.0
9	37.5	46.7	6.7	15.2	5.1	6.1
10	41.3	50.0	5.7	7.5	2.4	3.1
11	90.1	111.2	5.6	14.5	1.6	2.3
12	19.9	24.3	2.0	3.3	1.8	2.4
13	31.7	39.1	3.5	7.0	2.6	3.5
14	105.6	128.6	7.8	9.8	3.3	6.1
15	97.9	121.5	5.9	7.3	2.4	4.2
Mean	47.7	59.0	6.3	10.8	3.3	4.8
σ	27.6	33.8	4.4	7.9	1.3	1.7
σ_m	1.8	2.3	0.3	0.5	0.1	0.1

height, and slop angle were 3 cm, 2 cm, and 45^0-50^0, respectively. Two components of prism were gluing together as double-sided printing was not possible and it was printed on December, 2014. Photographs of prisms are shown in Fig. 5.4. Measured surface roughness of the 3D printed and glass moulded prisms without and with filter are shown in Tables 5.5, and 5.6, and in Tables 5.7, and 5.8, respectively. The quality of glass moulded prism is better than 3D printed prism. However, glass moulded prism can be used in imaging after polishing. Photographs of 3D printed and glass

TABLE 5.2

Surface roughness of the 3D printed flat sample B, where σ and σ_m are the standard deviation and mean of the standard deviation, respectively.

Evaluation area in μm^2	Roughness in nm without filter					
	622×467		125×94		62×47	
Number of observation	δ_a	δ_q	δ_a	δ_q	δ_a	δ_q
1	60.7	73.5	6.5	8.7	2.4	3.2
2	48.0	57.9	4.6	5.7	2.3	3.6
3	20.7	26.9	29.1	55.6	5.2	7.1
4	48.2	58.2	2.5	3.5	2.9	3.6
5	28.7	37.2	5.2	6.7	2.8	4.0
6	37.2	46.4	7.0	8.4	3.5	4.8
7	74.6	91.1	8.4	10.4	3.2	4.2
8	57.7	70.3	4.3	5.8	3.4	4.2
9	13.5	16.9	2.9	5.3	2.1	3.0
10	54.7	67.6	13.0	21.7	2.3	2.9
11	44.2	54.6	3.6	4.6	2.5	3.6
12	68.5	83.1	2.4	3.3	2.6	3.7
13	18.0	22.7	3.8	4.8	2.4	3.9
14	40.1	49.5	3.2	4.5	2.0	2.6
15	37.1	45.3	2.8	4.1	5.1	8.2
Mean	43.5	53.4	6.6	10.2	3.0	4.2
σ	18.2	21.7	6.8	13.4	1.0	1.5
σ_m	1.2	1.5	0.5	0.9	0.1	0.1

moulded prism surfaces by WYKO are shown in Figs. 5.5 and 5.6. Although the quality of 3D printed flat samples are better than 3D printed tilt and curve surfaces (e.g., prism).

TABLE 5.3

Surface roughness of the 3D printed flat sample A, where σ and σ_m are the standard deviation and mean of the standard deviation, respectively.

Evaluation area in μm^2	Roughness nm with filter					
	622×467		125×94		62×47	
Number of observation	δ_a	δ_q	δ_a	δ_q	δ_a	δ_q
1	12.2	20.5	4.5	9.3	2.5	5.3
2	9.0	15.0	12.9	29.6	4.1	5.8
3	9.2	14.8	4.0	12.7	3.5	4.9
4	12.8	21.7	3.6	4.8	6.0	8.1
5	4.9	8.6	3.2	4.4	4.0	5.2
6	7.6	12.3	3.4	7.9	3.5	6.2
7	8.4	13.5	7.2	10.0	2.2	3.0
8	7.9	12.6	6.4	8.0	3.9	4.9
9	6.5	12.1	5.2	14.3	5.0	6.0
10	8.1	12.2	5.3	7.0	2.3	3.0
11	13.1	26.0	3.4	15.6	1.6	2.3
12	3.9	6.7	1.8	3.0	1.8	2.4
13	5.1	9.3	3.1	6.7	2.6	3.5
14	16.4	30.6	4.4	6.1	3.3	6.1
15	17.1	25.2	3.6	4.9	2.4	4.2
Mean	9.5	16.1	4.8	9.6	3.3	4.7
σ	4.0	7.1	2.6	6.7	1.2	1.7
σ_m	0.3	0.5	0.2	0.4	0.1	0.1

5.2 Surface waviness

The approximate length and height of 3D printed plano-convex lenses were 1 cm and 1-7 mm, respectively. Photographs of the 3D printed lenses are shown in Fig. 5.7. The surface waviness of 3D printed lenses and glass molded lenses were characterized qualitatively by using a 4F imaging setup. The schematic of the 4F imaging setup is shown in Fig. 5.8. Thorlabs [39] grid array R1L353 was used as a test grid. The

TABLE 5.4

Surface roughness of the 3D printed flat sample B, where σ and σ_m are the standard deviation and mean of the standard deviation, respectively.

Evaluation area in μm^2	Roughness in nm with filter					
	622×467		125×94		62×47	
Number of observation	δ_a	δ_q	δ_a	δ_q	δ_a	δ_q
1	8.0	15.8	5.1	7.3	2.3	3.1
2	6.3	12.6	3.2	4.1	2.2	3.6
3	8.1	13.4	19.3	44.6	5.0	6.9
4	9.7	16.8	2.2	3.2	2.8	3.5
5	5.8	10.2	3.9	5.2	2.8	4.0
6	7.0	12.5	4.5	5.6	3.3	4.6
7	11.5	22.1	5.7	7.1	3.1	4.1
8	12.4	20.9	3.6	5.0	3.2	4.0
9	4.4	7.1	2.6	5.0	2.0	2.9
10	8.5	15.8	8.3	16.2	2.3	2.9
11	9.7	16.6	2.6	3.5	2.5	3.5
12	11.4	21.2	2.1	2.9	2.6	3.7
13	5.4	8.2	3.4	4.3	2.4	3.8
14	6.3	11.5	2.9	4.0	1.9	2.5
15	6.1	10.7	2.6	3.8	5.0	8.2
Mean	8.0	14.4	4.8	8.1	2.9	4.1
σ	2.5	4.7	4.3	10.6	1.0	1.5
σ_m	0.2	0.3	0.3	0.7	0.1	0.1

focal length of lens1 and lens2 were F_1 and F_2, respectively. When a light source illuminated the test grid, light from the grid was incident on lens1 and transmitted by it. After that, transmitted light was incident on lens2 and focused on the pixels of USB camera, which was connected with a computer. USB camera was placed at the focal point of lens2. In the reference measurement lens1 and lens2 were Thorlabs normal glass lens. In the actual measurement lens2 was replaced by the 3D printed lens. The image quality of the test grid through 3D printed and glass lens at different

TABLE 5.5

Surface roughness of the prisms for surface 1 without filter, where σ and σ_m are the standard deviation and mean of the standard deviation, respectively.

Evaluation area in μm^2	Roughness of 3D printed in nm				Roughness of glass moulded in nm			
	622×467		125×94		622×467		125×94	
Number of observation	δ_a	δ_q	δ_a	δ_q	δ_a	δ_q	δ_a	δ_q
1	207.6	255.5	34.4	41.9	58.7	75.6	24.6	29.8
2	269.4	335.1	19.9	27.7	91.7	120.8	27.5	34.8
3	243.1	293.2	16.0	19.9	50.9	65.5	18.4	25.7
4	180.7	237.8	27.2	33.8	54.3	68.1	17.8	21.7
5	190.6	242.9	27.4	34.0	53.8	68.9	19.2	26.1
6	177.4	224.2	21.0	27.4	41.0	52.4	11.4	13.7
7	180.9	235.8	21.3	26.3	48.5	63.2	15.5	19.7
8	123.9	157.0	22.0	26.7	67.9	86.5	9.6	12.2
9	136.9	158.7	20.5	27.9	56.4	73.3	10.7	13.0
10	342.4	465.6	38.5	51.1	42.9	55.8	15.4	20.5
Mean	205.3	260.6	24.8	31.7	56.6	73.0	17.0	21.7
σ	64.8	89.8	7.1	9.0	14.6	19.4	5.8	7.5
σ_m	6.5	9.0	0.7	0.9	1.5	1.9	0.6	0.8

focal lengths are shown from Figs. 5.9 to 5.11. The images of the test grid by 3D printed lenses were consisted with waviness and it comes from the manufacturing process.

5.3 Scattering

The scattering measurement setups are shown in Figs. 5.12 and 5.13. Light from the laser is incident on a lens. Light transmitted by the lens was observed on the screen. The transmitted light was scattered because of surface structures. Scattered light was captured by a camera. Both of 3D printed short and long focal length lenses were measured. Then scattering by reference lens (glass lens by Thorlabs) was observed. The quality of the lens is poor or good if scattering is high or low,

TABLE 5.6

Surface roughness of the prisms for surface 2 without filter, where σ ,σ_m are the standard deviation and mean of the standard deviation, respectively).

	Roughness of 3D printed in nm				Roughness of glass moulded in nm			
Evaluation area in μm^2	622×467		125×94		622×467		125×94	
Number of observation	δ_a	δ_q	δ_a	δ_q	δ_a	δ_q	δ_a	δ_q
1	126.9	170.3	55.4	67.4	90.5	115.2	22.7	28.4
2	136.3	163.3	50.5	62.3	101.4	127.5	36.5	43.3
3	176.5	236.1	25.1	32.6	103.2	130.3	39.1	47.7
4	157.9	214.1	26.8	35.3	112.6	131.8	30.8	38.2
5	153.2	188.7	65.4	80.8	102.3	129.9	23.6	29.0
6	138.8	182.1	57.1	66.3	91.7	113.2	16.2	20.3
7	175.2	218.4	51.6	69.0	67.7	87.2	18.8	23.1
8	108.9	139.0	67.1	62.4	64.8	87.3	27.8	32.0
9	165.5	220.4	64.3	85.4	88.8	111.3	40.1	46.9
10	159.3	215.4	48.1	76.4	100.5	124.5	28.7	37.9
Mean	149.8	194.8	51.1	63.7	92.4	115.8	28.4	34.7
σ	21.8	30.9	14.8	17.5	15.5	16.7	8.3	9.6
σ_m	2.2	3.1	1.5	1.8	1.6	1.7	0.8	1.0

respectively. Photographs of scattering measurements are shown from Figs. 5.14 to 5.16. The scattering of 3D printed lens was high compared to reference lens. The light scattered by 3D printed lens was non-uniform because the surface of 3D printed lenses consisted of gratings that was observed in between scattered light.

TABLE 5.7

Surface roughness of the prisms for surface 1 with filter, where σ and σ_m are the standard deviation and mean of the standard deviation, respectively.

Evaluation area in μm^2	Roughness of 3D printed in nm				Roughness of glass moulded in nm			
	622×467		125×94		622×467		125×94	
Number of observation	δ_a	δ_q	δ_a	δ_q	δ_a	δ_q	δ_a	δ_q
1	102.2	129.9	17.3	23.4	12.5	18.3	13.9	17.6
2	101.8	146.9	13.2	17.6	18.5	33.4	14.5	19.5
3	97.4	133.2	9.8	12.4	14.3	21.4	13.8	19.0
4	83.4	123.3	13.8	18.6	11.4	16.3	11.4	14.8
5	85.1	125.2	16.7	21.6	10.4	14.9	13.4	18.4
6	91.4	123.7	13.5	18.2	9.4	13.8	6.7	8.5
7	92.2	126.6	12.5	16.2	11.3	16.9	9.0	11.7
8	66.9	89.1	13.6	17.2	12.6	20.6	6.6	8.8
9	69.1	88.3	12.4	19.2	12.2	22.0	6.5	8.2
10	170.9	244.9	24.0	35.3	9.1	14.0	9.5	13.9
Mean	96.0	133.1	14.7	20.0	12.2	19.2	10.5	14.0
σ	29.0	43.4	3.9	6.2	2.7	5.8	3.3	4.5
σ_m	2.9	4.3	0.4	0.6	0.3	0.6	0.3	0.5

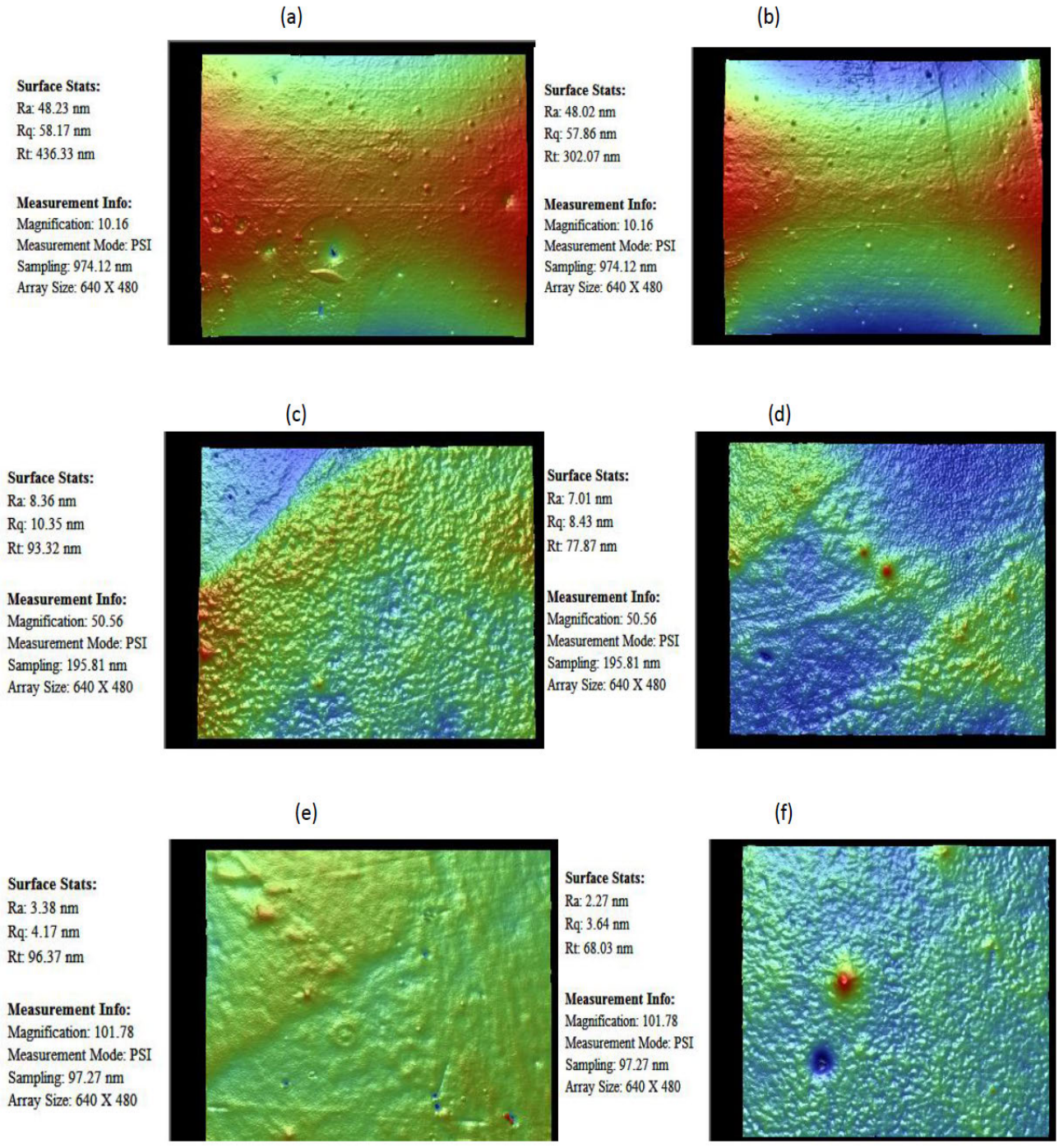

Figure 5.3: Photographs of 3D printed flat sample B by WYKO NT9300 at evaluation area (a,b) 622×467 μm^2, (c,d) 125×94 μm^2, and (e,f) 62×47 μm^2.

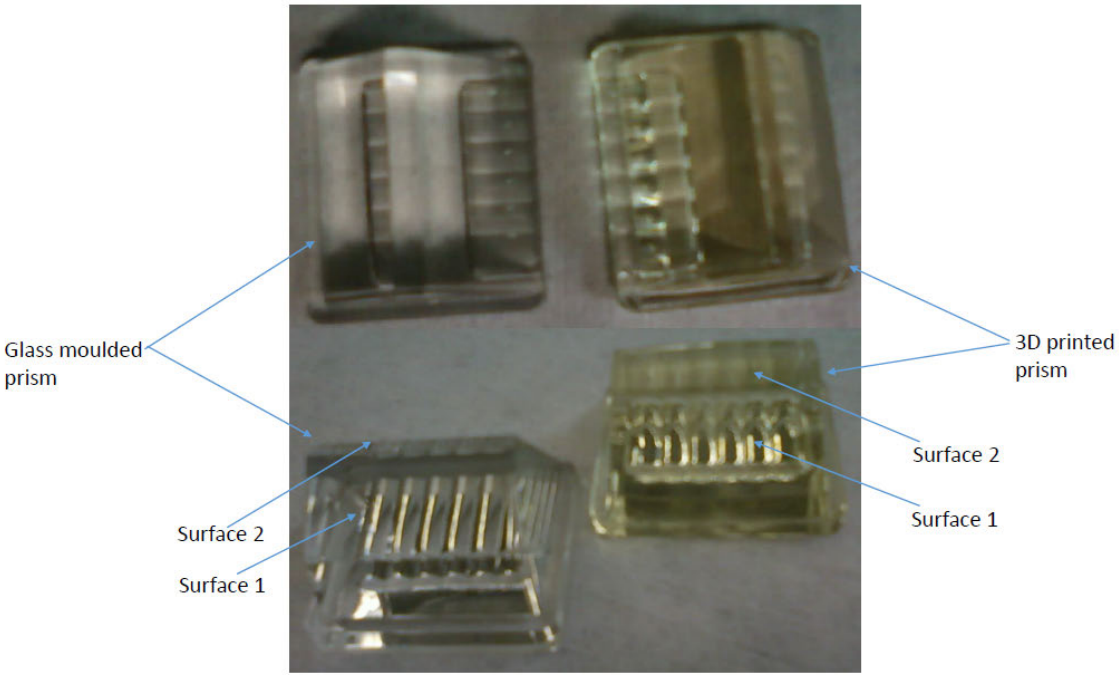

Figure 5.4: Photographs of prisms.

TABLE 5.8

Surface roughness of the prisms for surface 2 with filter, where σ ,σ_m are the standard deviation and mean of the standard deviation, respectively.

	Roughness of 3D printed in nm				Roughness of glass moulded in nm			
Evaluation area in μm^2	622×467		125×94		622×467		125×94	
Number of observation	δ_a	δ_q	δ_a	δ_q	δ_a	δ_q	δ_a	δ_q
1	94.6	141.3	33.5	42.0	23.6	35.4	15.4	19.8
2	78.1	97.4	29.2	36.7	23.5	34.8	18.4	22.5
3	86.4	144.5	18.1	24.5	23.3	34.6	21.0	25.9
4	91.4	135.6	17.5	23.4	21.1	29.6	18.4	24.2
5	91.4	116.6	43.3	55.9	18.3	32.2	13.1	17.5
6	99.1	129.8	29.3	46.9	17.4	26.0	10.7	14.1
7	103.5	137.8	29.1	39.1	15.2	22.5	11.9	15.7
8	78.9	99.2	26.4	33.9	17.0	26.0	15.8	18.9
9	112.5	158.1	33.1	46.1	17.2	24.5	22.1	28.6
10	87.5	124.3	33.7	42.4	18.3	26.5	18.8	26.8
Mean	92.3	128.5	29.3	39.1	19.5	29.2	16.5	21.4
σ	10.7	19.5	7.6	10.0	3.1	4.8	3.8	5.0
σ_m	1.1	2.0	0.8	1.0	0.3	0.5	0.4	0.5

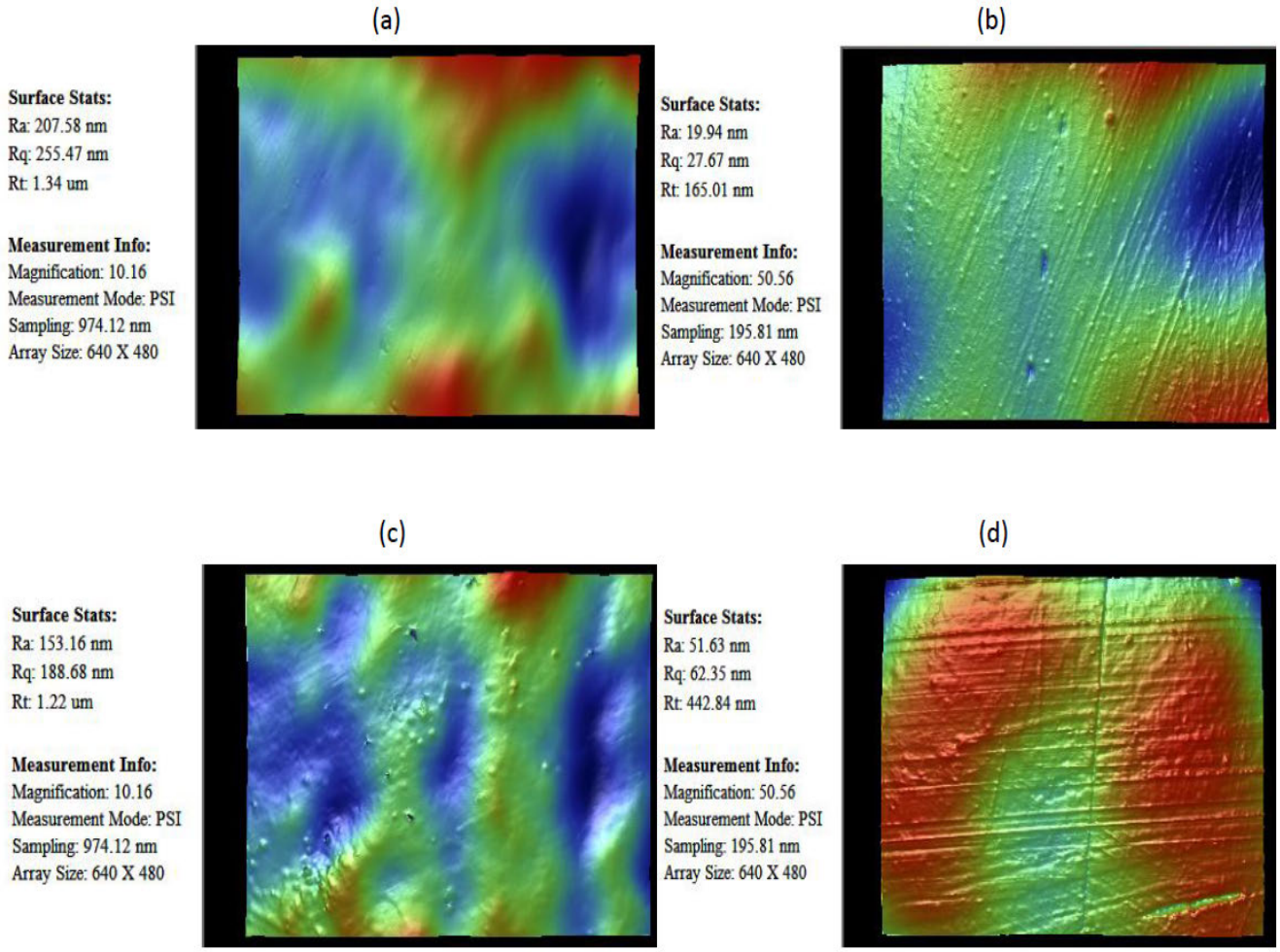

Figure 5.5: Photographs of (a,b) 3D printed prism surface 1 and (c,d) 3D printed prism surface 2 by WYKO NT9300.

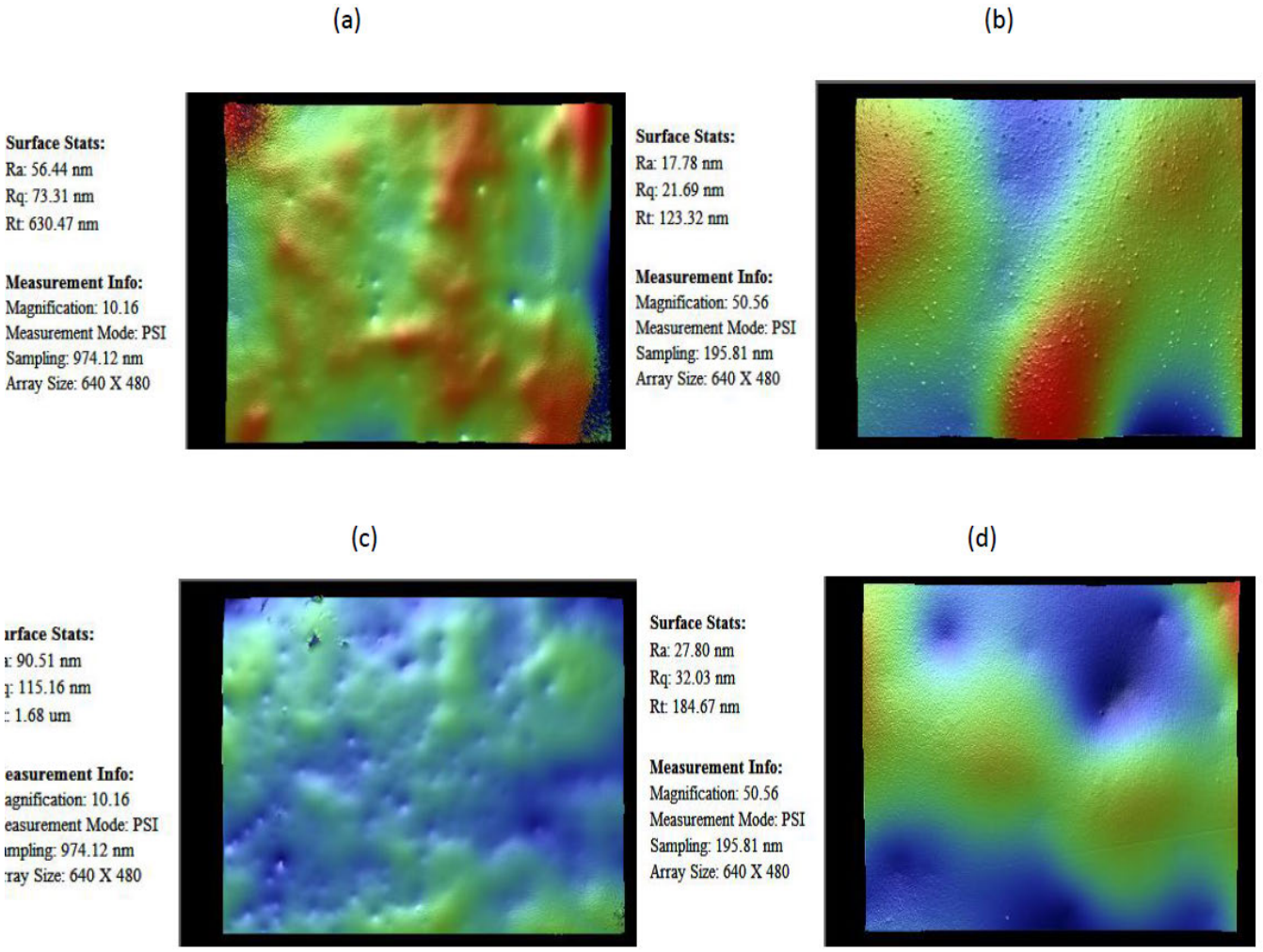

Figure 5.6: Photographs of (a,b) glass moulded prism surface 1 and (c,d) glass moulded prism surface 2 by WYKO NT9300.

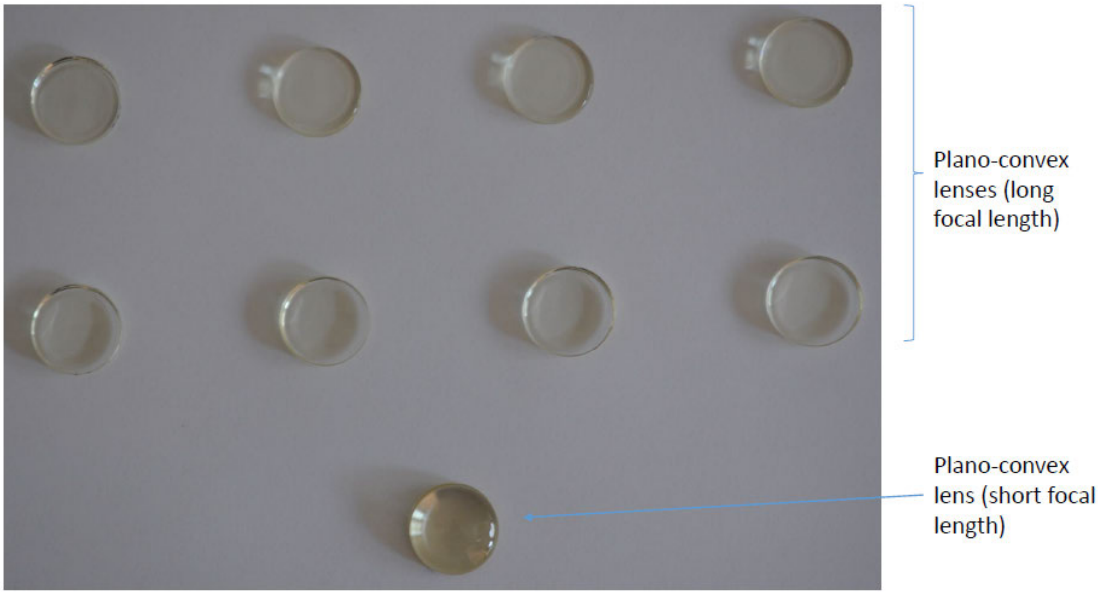

Figure 5.7: Photographs of the 3D printed plano-convex lenses.

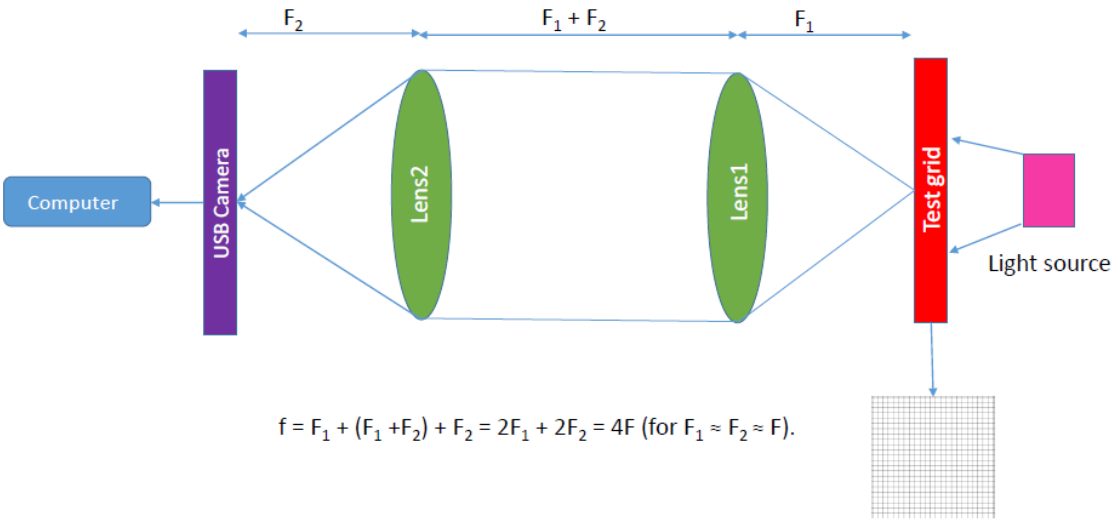

Figure 5.8: Schematic of a 4F imaging setup.

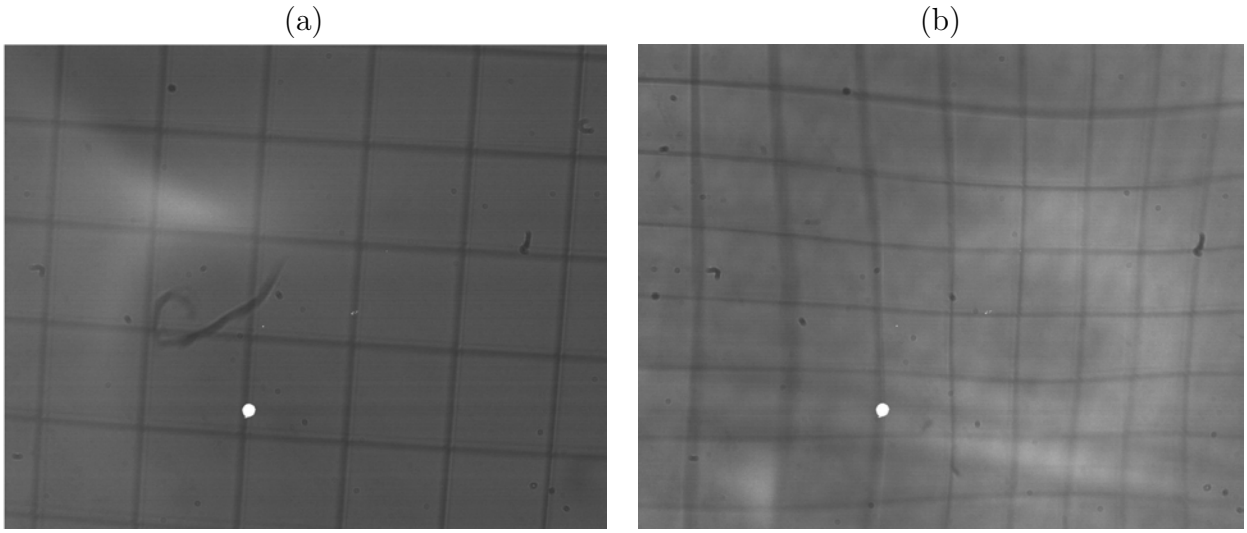

Figure 5.9: Image quality of the test grid by (a) glass lens with focal length 25 mm and (b) 3D printed lens with focal length 30 mm.

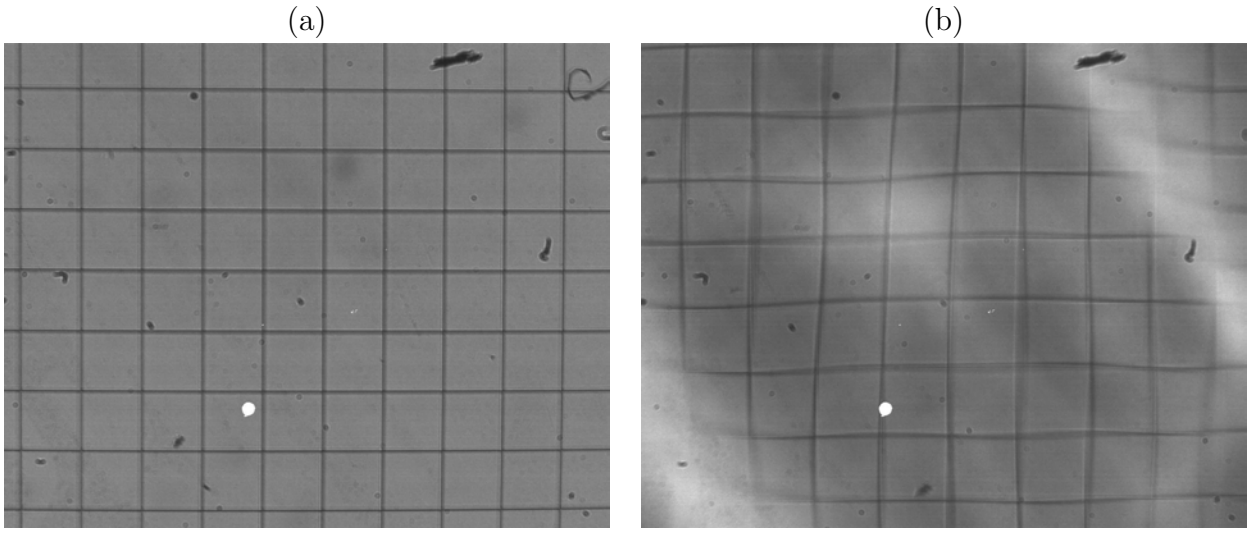

Figure 5.10: Image quality of the test grid by (a) glass lens and (b) 3D printed lens with focal length 75 mm.

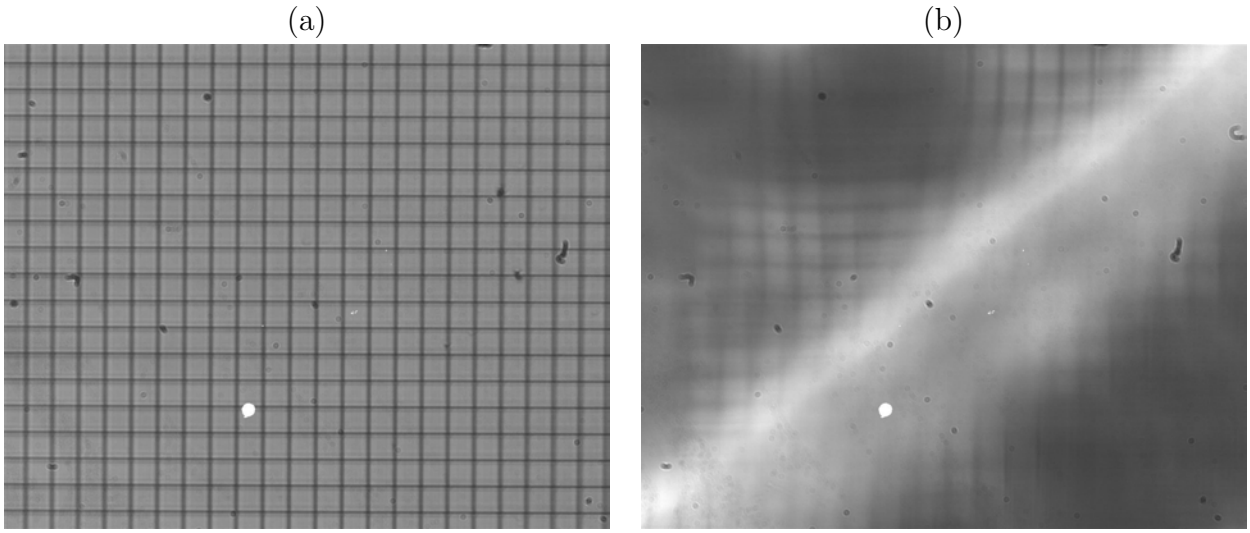

Figure 5.11: Image quality of the test grid by (a) glass lens (b) 3D printed lens with focal length 20 cm.

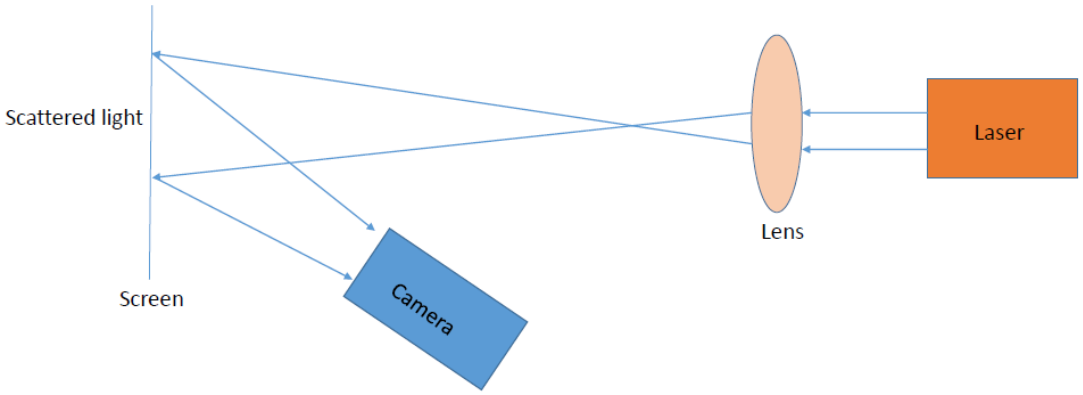

Figure 5.12: Schematic of the scattering measurement setup (short focal length lens).

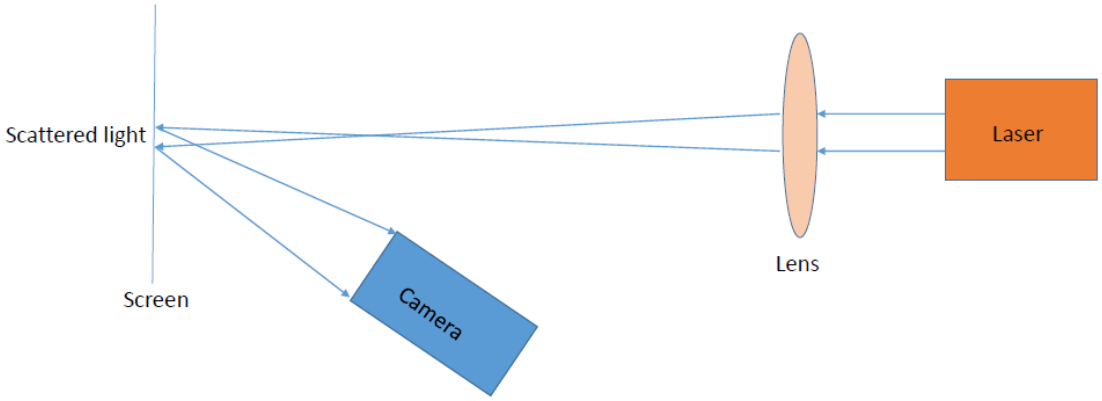

Figure 5.13: Schematic of the scattering measurement setup (long focal length lens).

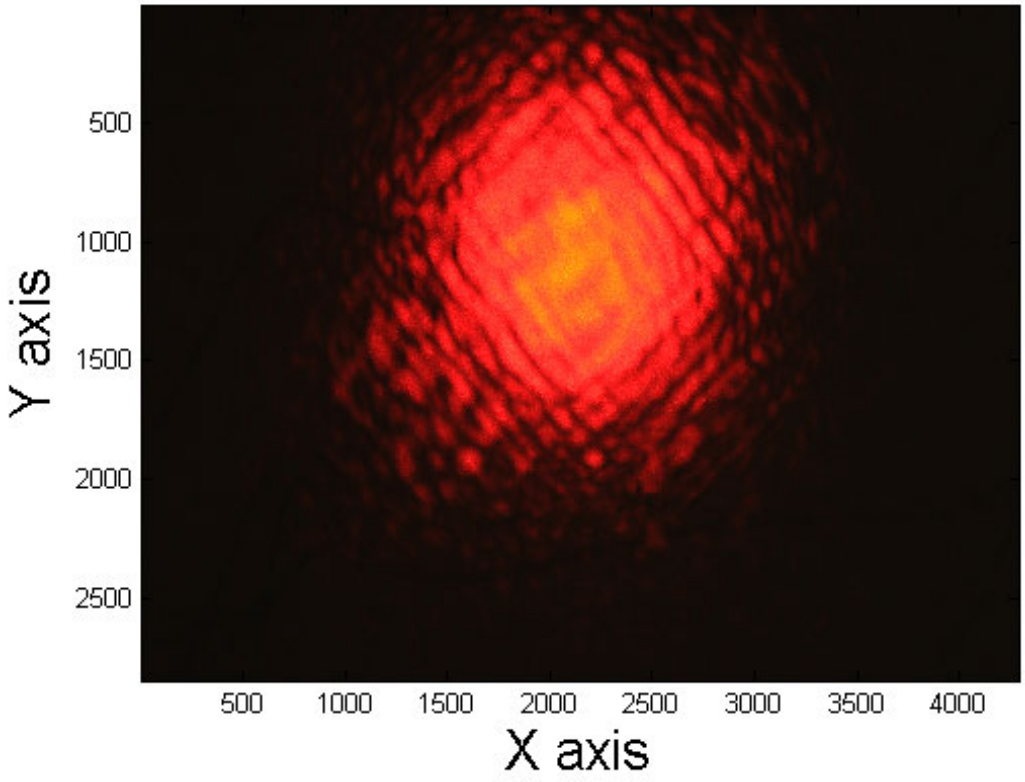

Figure 5.14: Scattering by 3D printed lens of focal length 30 mm.

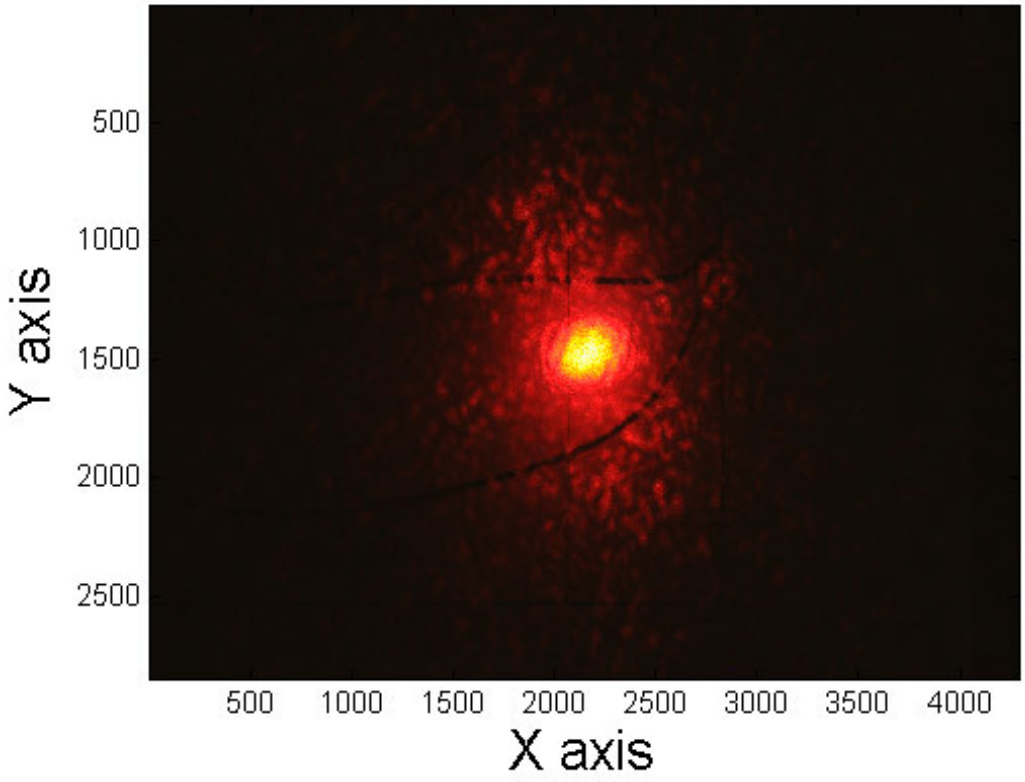

Figure 5.15: Scattering by 3D printed lens of focal length 20 cm.

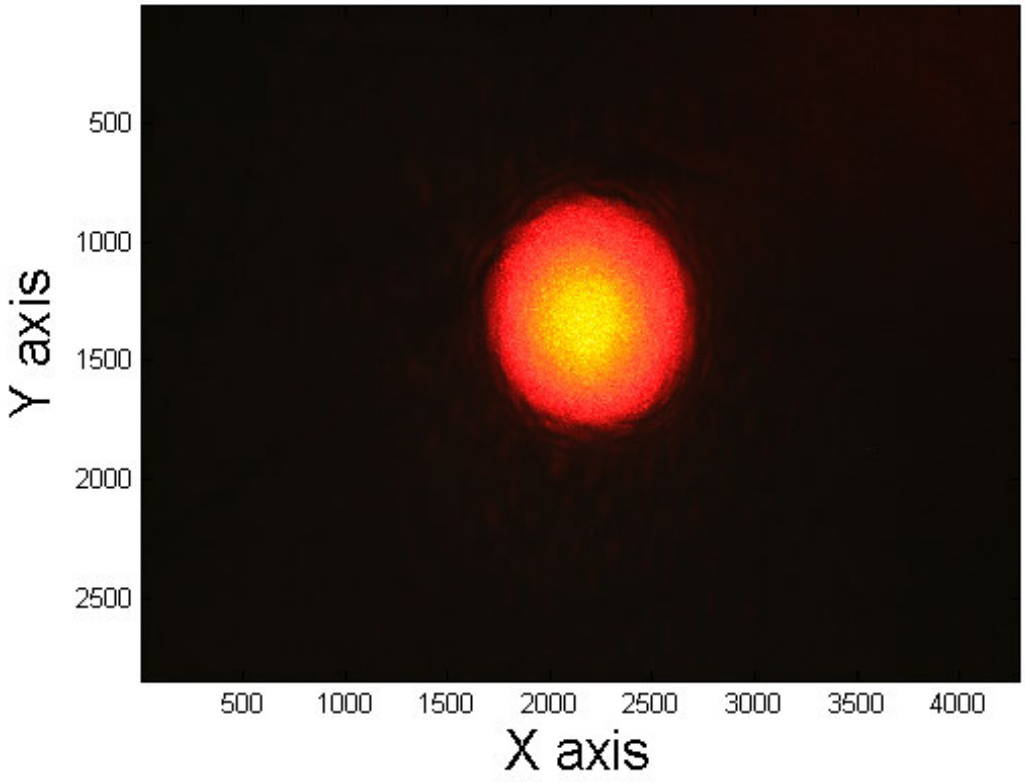

Figure 5.16: Scattering by the reference lens with focal length 25 mm.

Chapter VI

Conclusions

The surface roughness of 3D printed and moulded glass optics by Oplatek were measured successfully by optical profilometer. The surface waviness and scattering of 3D printed and glass optics by Thorlab were measured by a 4F imaging and scattering measurement setup respectively. The waviness on surface was high: surface roughness value was increased with evaluation area. The surface roughness value was diminished from the surface by filtering that improved surface roughness. The 3D printed surface rms roughness within evaluation area 62×47 μm^2 was 24 nm by LUXeXceL′s previous generation equipment. But now with next generation equipment it is close to 5 nm (62×47 μm^2). The 3D printed optics by LUXeXceL's previous generation equipment consisted with point defects such as bumps, nipples, and snowflakes, but now with LUXeXceL's next generation equipment, all point defects are removed. Currently, the quality of 3D printed surface is close to imaging optics. From these measurements it can conclude that the 3D printed optics from LUXeXceL′s next generation equipment is improved.

The surface rms roughness of unpolished 3D printed and glass moulded prisms were also checked. There values were close to each other. It shows that without polishing surface of 3D printed and glass moulded prisms consists with waviness. Although the quality of glass moulded prism is better than 3D printed prism. Surface rms roughness was decreased when waviness was removed by filter. From these measurements it can conclude that muolded optics can be used in imaging after polishing. Additionally, the quality of 3D printed flat surface is better than 3D printed tilt and curve surfaces (e.g., prism).

The surface waviness of 3D printed lenses were characterized visually by a 4F imaging setup and glass lens is used as a reference lens. Waviness was observed on test grid images that were formed by 3D printed lens. From this measurement, it can conclude that the waviness came from the manufacturing process.

The scattering by 3D printed lenses were observed. Light scattered by 3D printed lenses were high compared to the reference glass lens. The 3D printed lenses consisted of grating that was observed in between scattered light. Grating comes from the manufacturing process. From this measurement it can conclude that if waviness are removed from the 3D printed sample then it can be used in future for imaging.

Chapter VII

Future work

Currently, 3D printed optics is close to imaging optics. It can be used for imaging if surface waviness is improved. The 3D printed surface quality can be improved in future by solving following issues:

- Good surface quality of 3D printed optics needs smooth enough drop. The drop with smooth surface can be achieved by selecting material with low viscosity.
- Poor contact angle between drop and substrate decreases the surface quality of 3D printed optics. The contact angle is good enough if the surface free energy of printing medium is much higher than the surface tension of the 3D printable material.
- 3D printable material with low density causes spattering of drop on substrate that decrease the surface quality. Material with high density prevents the spattering effect.
- Surface quality of 3D printed optics can be improved by reducing a drop diameter from μm to nm region. In present drop diameter in μm region is possible (see Section 3.2). If nozzle diameter in nm region is achieved, then drop diameter in nm region may be possible. But, in practice, nozzle diameter in nm region is difficult to achieve. Smaller drop from a larger nozzle can be created by electrohydrodynamic (EHD), cavity collapse, and acoustic inkjet printing technology. Additionally, nano droplets will not be deposited at proper position because of the air turbulence effect. Vacuum environment can prevents such effects.

- Surface quality of 3D printed optics can be improved by depositing drop at proper position (see Section 3.3.2).

Bibliography

[1] F. R. S. Rayleigh, "On the instability of jets," *Proc. London Math. Soc.* **10(4)**, 4–13 (1878).

[2] R. Elmqvist, "Measuring instrument of the recording type," *US Patent no.* **2**, 566,443 (1948).

[3] R. G. Sweet, "Signal apparatus with fluid drop recorder," *US Patent no.* **3**, 596,275 (1971).

[4] P. Calvert, "Inkjet printing for materials and devices," *Chem. Matter* **13**, 3299–3305 (2001).

[5] B. G. Levi, "New printing technologies raise hopes for cheap plastic electronics," *Phys. Today* **54**, 2–20 (2001).

[6] LUXeXceL, `http://www.luxexcel.com/` (valid 10.04.2015).

[7] B. K. Jocelyn, "Characterization of 3D printed optical components, Master of Science Thesis," *University of Eastern Finland* (2014).

[8] Oplatek, `http://www.oplatek.com/` (valid 12.04.2015).

[9] J. J. Beaman, J. W. Barlow, D. L. Bourell, R. H. Crawford, H. L. Marcus, and K. P. Mcalea, "Solid freeform fabrication: A new direction in manufacturing," *Massachusetts: Kluwer academic publishers,* 1-49 and 121-165 (1997).

[10] M. K. Agarwala, A. Bandyopadhyay, R. v. Weeren, N. A. Langrana, A. Safari, S. C. Danforth, V. R. Jamalabad, P. J. Whalen, R. Donaldson, and J. Pollinger,

"Fused deposition of ceramics (FDC) for structural silicon nitride components," *Proc. solid freeform fabrication symposium, University of Texas at Austin,* 326-334 (Aug. 1996).

[11] J. G. Conley and H. L. Marcus, "Rapid prototyping and solid free form fabrication," *J. Manuf. Sci. Engrg.-Trans. ASME* **119(4B)**, 811–816 (1997).

[12] M. L. Griffith and J. W. Halloran, "Freeform fabrication of ceramics via stereolithography," *J. Am. Ceram. Soc.* **79(10)**, 2601–2608 (1996).

[13] H. P. Le, "Progress and trends in ink-jet printing technology," *J. Imaging Sci. Tech.* **42(1)**, 49–62 (1998).

[14] B. Y. Tay, "Continuous direct ink-jet printing, Doctor of Philosophy Thesis," *Queen Mary, University of London, Department of Materials* (July, 2001).

[15] J. Brünahl and A. M. Grishin, "Piezoelectric shear mode drop-on-demand inkjet actuator," *Sensors and Actuators A* **101**, 371–382 (2002).

[16] E. L. Kyser and S. B. Sears, "Method and apparatus for recording with writing fluids and drop projection means thereof," *US patent no.* **3**, 946,398, to Silonics Inc. (1976).

[17] G. I. Taylor, "Disintegration of water drops in an electric field," *Proc. of the royal society of london series A. mathematical and physical sciences* **280(1382)**, 383–397 (1964).

[18] J. Zeleny, "Instability of electrified liquid surfaces," *Physical review* **10(1)**, 1–7 (1917).

[19] C. R. Winston, "Method and apparatus for transferring ink," *US Patent* **3**, 060429 (1962).

[20] J. R. Castrejón-Pita, W. R. S. Baxter, J. Morgan, S. Temple, G. D. Martin, and I. M. Hutchings, "Future, opportunities and challenges of inkjet technologies," *Atomization and sprays* (2013).

[21] A. A. Castrejon-Pita, J. R. Castrejon-Pita, and G. D. Martin, "A novel method to produce small droplets from large nozzles," *Review of scientific instruments* **83(11)**, 115105 (2012).

[22] S. Gekle and J. M. Gordillo, "Generation and breakup of Worthington jets after cavity collapse. Part 1. Jet formation," *Journal of fluid mechanics* **663**, 293–330 (2010).

[23] B. Hadimioglu, S. A. Elrod, D. L. Steinmetz, M. Lim, J. C. Zesch, B. T. Khuri-Yakub, E. G. Rawson, and C. F. Quate, "Acoustic ink printing," *Ultrasonics Symposium* 929 (1992).

[24] J. E. Fromm, "Numerical-calculation of the fluid-dynamics of drop-on-demand jets," *IBM 7. Res. Dev.* **28**, 322–333 (1984).

[25] N. Reis and B. Derby, "Ink jet deposition of ceramic suspensions: modelling and experiments of droplet formation," *MRS Symp. proc.* **624**, 65–70 (2000).

[26] C. D. Stow and M. G. Hadfield, "An experimental investigation of fluid-flow resulting from the impact of a water drop with an unyielding dry surface," *Proc. R. Soc. London Ser. A* **373**, 419–441 (1981).

[27] R. Bhola and S. Chandra, "Parameters controlling solidification of molten wax droplets falling on a solid surface," *Mater. Sci.* **34**, 4883–4894 (1999).

[28] A. L. Yarin, "Drop impact dynamics: splashing, spreading, receding, bouncing," *Annu. Rev. Fluid Mecb.* **38**, 159–192 (2006).

[29] R. Rioboo, M. Marengo, and C. Tropea, "Time evolution of liquid drop impact onto solid, dry surfaces," *Exp. Fluids* **33**, 112–124 (2002).

[30] L. H. Tanner, "Spreading of silicone oil droplets on horizontal surfaces," *Phys. D Appl. Phys.* **12**, 1473–1484 (1979).

[31] B. Derby, "Inkjet printing of functional and structural materials: Fluid property requirements, feature stability, and resolution," *Annu. Rev. Mater. Res.* **40**, 395–414 (2010).

[32] S. H. Davis, "Moving contact lines and rivulet instabilities. 1. The static rivulet," *Fluid Mech.* **98**, 225–242 (1980).

[33] S. Schiaffino and A. A. Sonin, "Formation and stability of liquid and molten beads on a solid surface," *Fluid Mech.* **343**, 95–110 (1997).

[34] P. C. Duineveld, "The stability of ink-jet printed lines of liquid with zero receding contact angle on a homogeneous substrate," *Fluid Mech.* **477**, 175–200 (2003).

[35] D. Soltman and V. Subramanian, "Inkjet-printed line morphologies and temperature control of the coffee ring effect," *Langmuir* **24**, 2224–2231 (2008).

[36] R. De Vrie and B. Kurt, "Print-Optical Technology: Manufacture LED lenses by stacking droplets-on-demand," *LED Professional Review* **Issue 28**, 48–52 (Nov/Dec 2011).

[37] K. H. Guenther, P. G. Wierer, and J. M. Bennett, "Surface roughness measurements of low-scatter mirrors and roughness standards," *Applied Optics* **23**, 3821 (1984).

[38] U. Manual, "WYKO NT9800/9300 profiler, setup and operation guide," *Veeco Instruments Inc,* **USA** (2007).

[39] Thorlabs, `http://www.thorlabs.de/index.cfm?` (valid 27.06.2015).

Appendix A

Appendix

TABLE A.1
Symbols used in the Thesis.

Symbol	Significance
3D	Three-dimensional
Re	Reynolds number
We	Weber number
Oh	Ohnesorge number
B_0	Bond number
ρ	Density
η	Kinematic viscosity
γ	Surface tension
v	Velocity
v_{min}	Minimum velocity
$f(R)$	Function of surface roughness
a	Drop diameter
d_n	Nozzle diameter
d_{con}	Contact diameter
D	Lens diameter
g	Gravitational force
ξ_s	Surface free energy
ξ_{sl}	Interfacial tension between solid and liquid
θ	Contact angle
θ_{eqm}	Equilibrium contact angle
m	Meter
cm	Centimeter (10^{-2} m)
mm	Millimeter (10^{-3} m)
μm	Micro-meter (10^{-6} m)
nm	Nano-meter (10^{-9} m)

Symbol	Significance
t	Final time
t_0	Initial time
π	Pie
δ_q	Root-mean-square roughness
δ_a	Area roughness
σ	Standard deviation
σ_m	Mean of the standard deviation
λ	Wavelength
$\times$	Magnification
N	f/number
f	Focal length
UV	Ultraviolet
PSI	Phase-shifting-interferometry
VSI	Vertical-scan-interferometry

Appendix B

Appendix

(a)

(b)

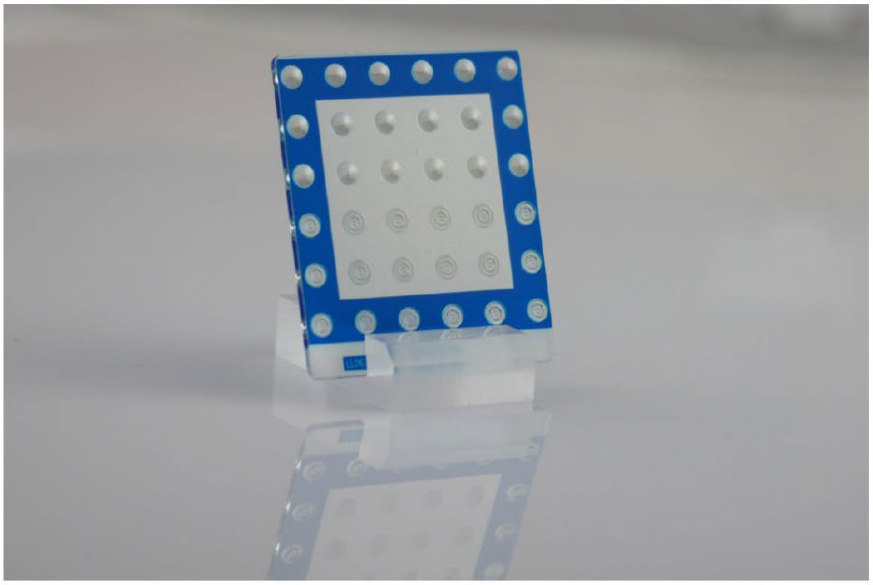

Figure B.1: Light Emitting Diode (LED) lens array [(a)table lamp)] and (b) multi lens array blue-white (copyright from LUXeXceL [6]).

(a)

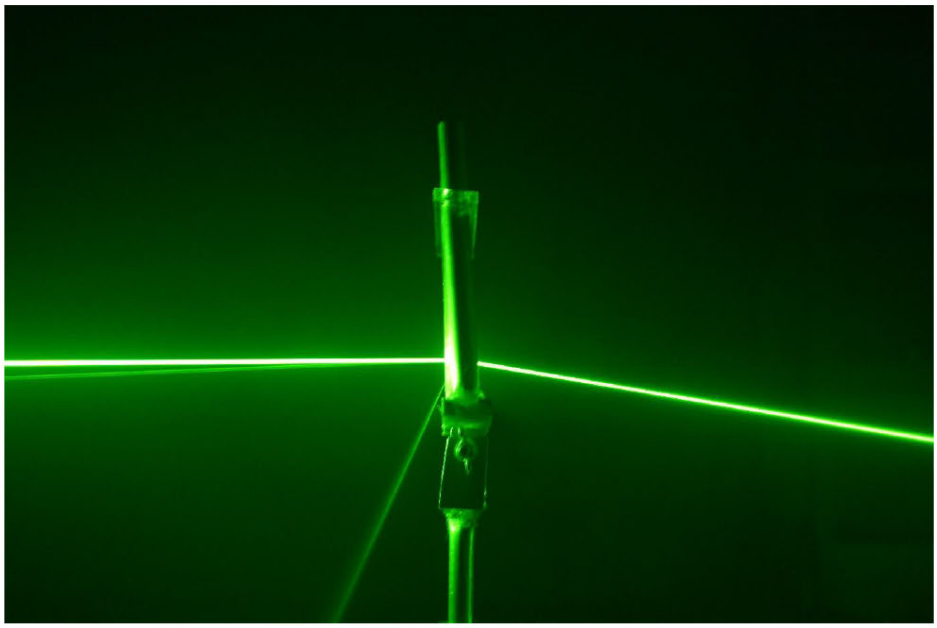

(b)

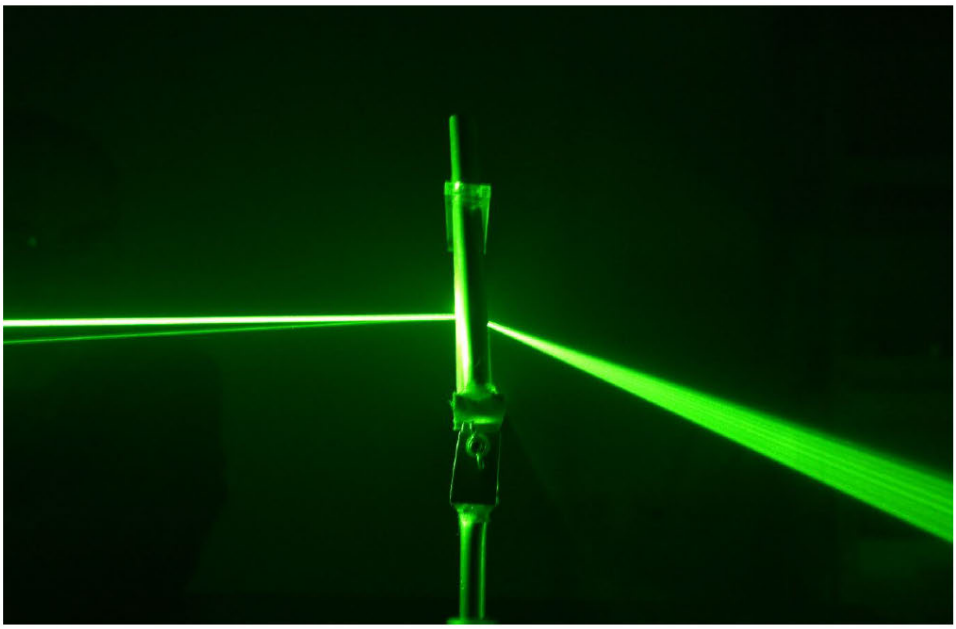

Figure B.2: (a) Large linear prism and (b) medium linear prism (copyright from LUXeXceL [6]).

(a)

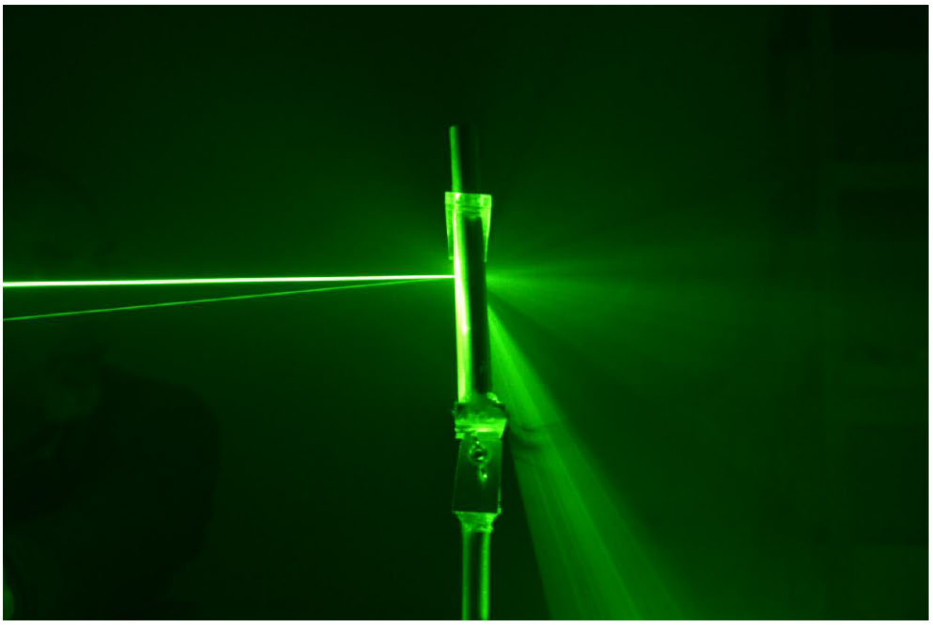

(b)

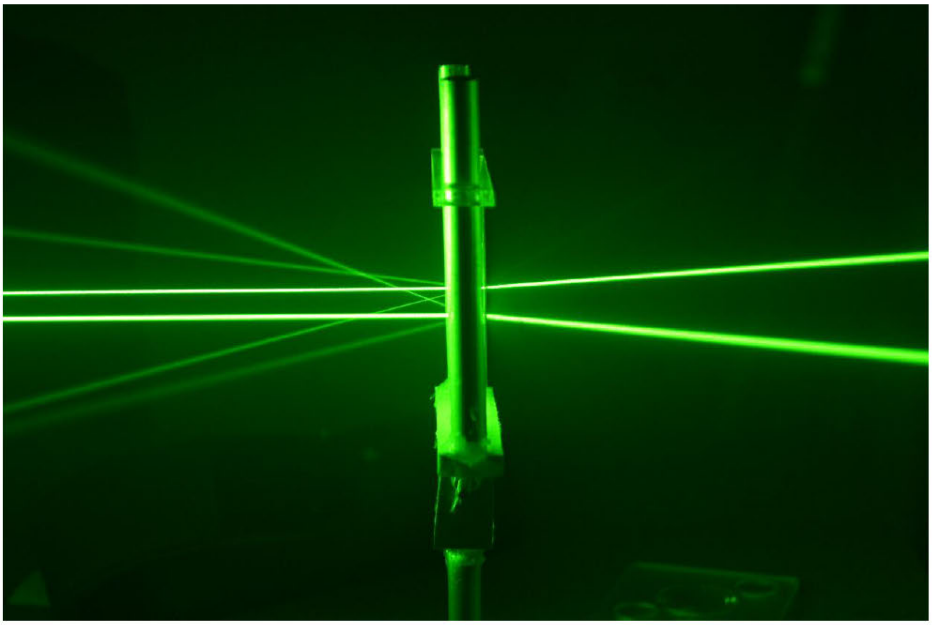

Figure B.3: (a) Small linear prism and (b) fresnel lens 1 (copyright from LUXeXceL [6]).

(a)

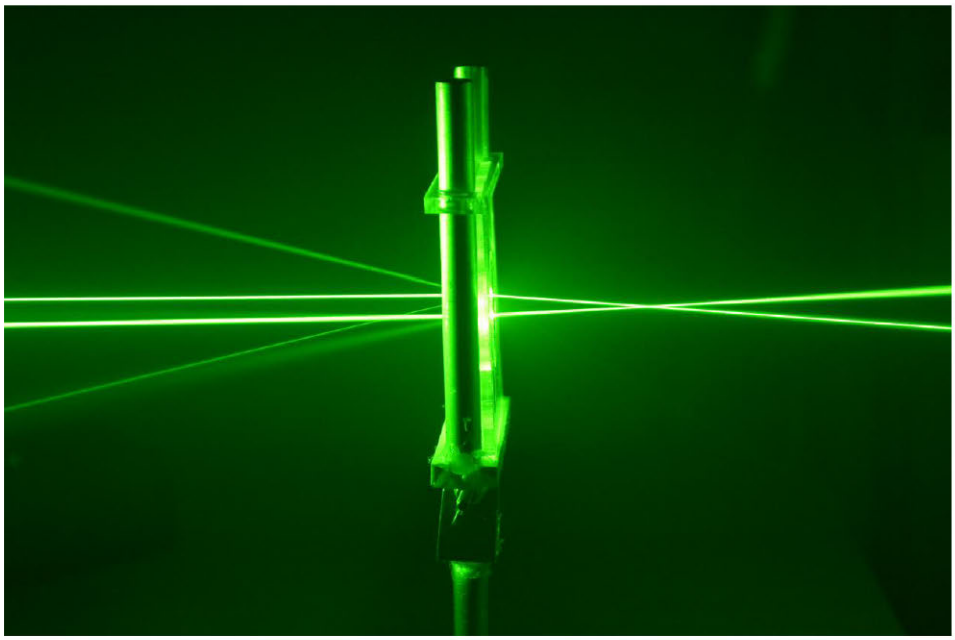

(b)

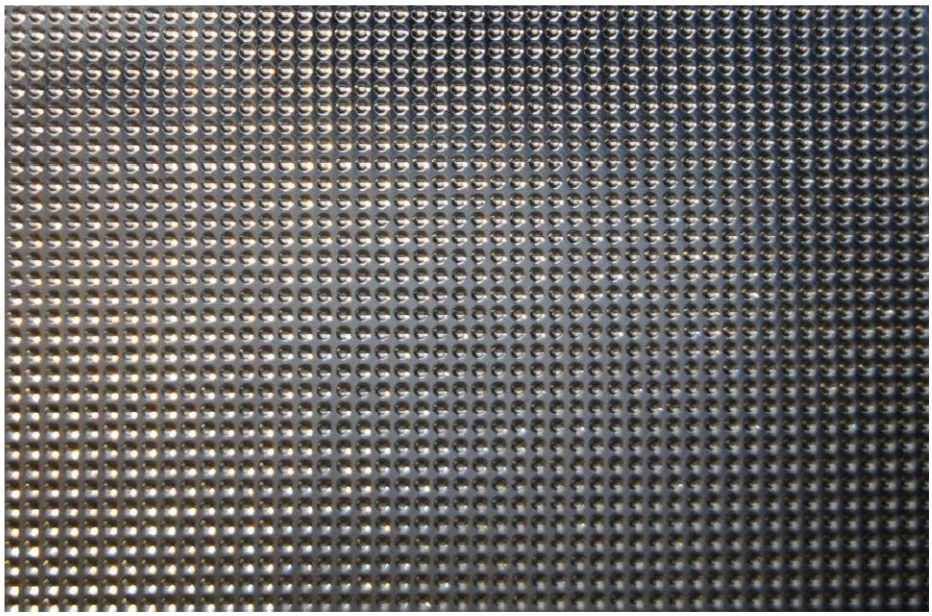

Figure B.4: (a) Fresnel lens 2 and (b) micro optics (copyright from LUXeX-ceL [6]).

(a)

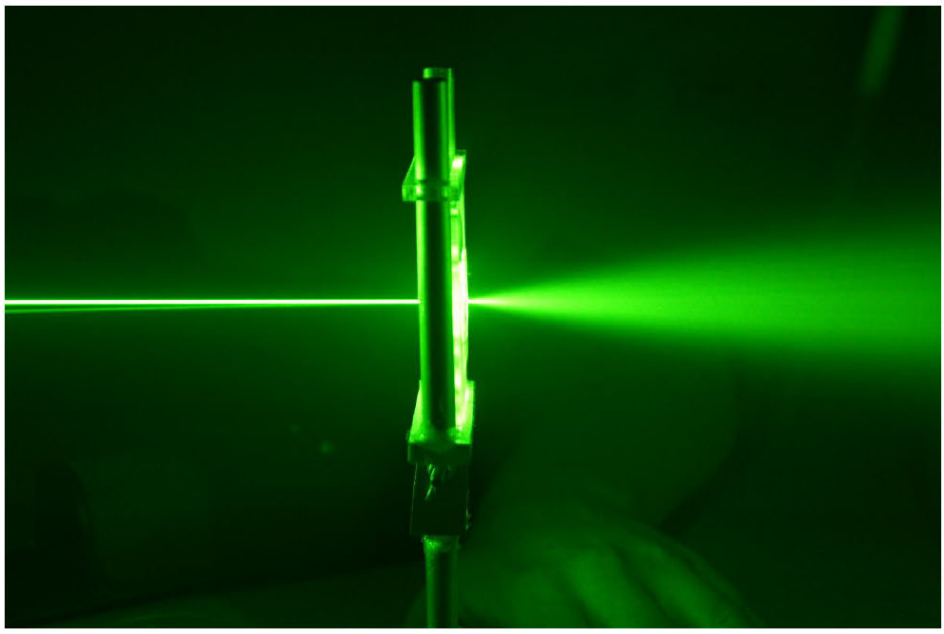

(b)

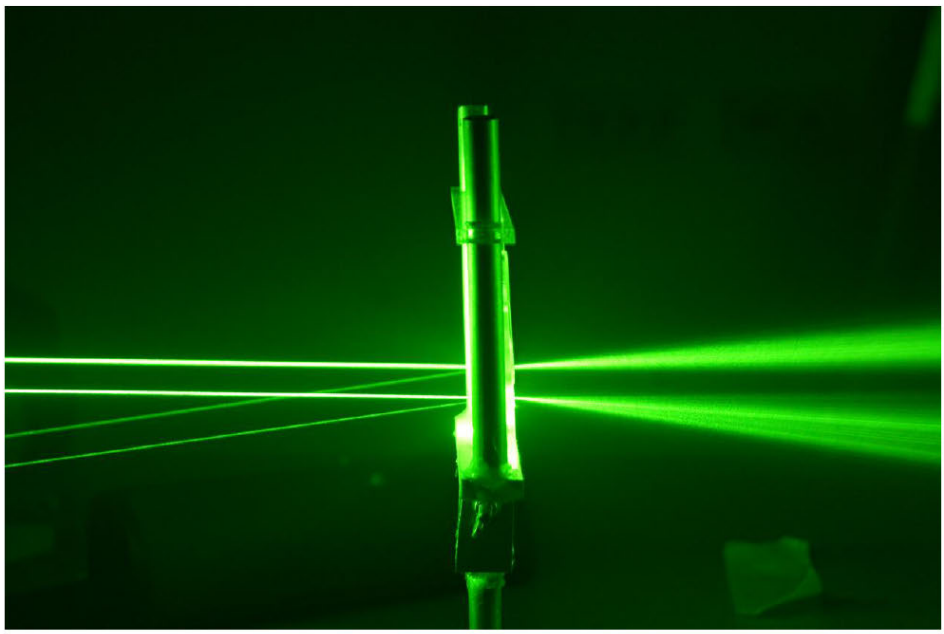

Figure B.5: (a) Spherical matte 1 and (b) spherical matte 2 (copyright from LUXeXceL [6]).

(a)

(b)

Figure B.6: (a) Sample 1 and (b) sample 2 (copyright from LUXeXceL [6]).